Spin dynamics simulations of classical ferro- and antiferromagnetic model systems: comparison with theory and experiment



1999 J. Phys.: Condens. Matter 11 R179

(http://iopscience.iop.org/0953-8984/11/18/201)

J. Phys.: Condens. Matter **11** (1999) R179–R213. Printed in the UK PII: S0953-8984(99)67858-4

**REVIEW ARTICLE**

# Spin dynamics simulations of classical ferro- and antiferromagnetic model systems: comparison with theory and experiment

D P Landau† and M Krech‡

† Center for Simulational Physics, The University of Georgia, Athens, GA 30602, USA
‡ Institut für Theoretische Physik, RWTH Aachen, 52056 Aachen, Germany

Received 24 August 1998

**Abstract.** In this article we review the progress which has been made in spin dynamics simulations of simple models of magnetic systems. We will describe modern spin dynamics methods and show results which have been obtained for a number of simple model systems. Where appropriate we will make comparison with experimental results and theoretical predictions.

## 1. Introduction

Although the static properties of a large number of physical systems have been well studied experimentally and many simple models have been examined by both theoretical and simulational means, the study of the dynamic properties of magnetic systems is far less mature. Arguably the most well developed simulational approach to these systems is the Monte Carlo method in its various versions. Unfortunately these techniques are fundamentally stochastic in nature and there is no correlation between the development of a system in *Monte Carlo time* and in *real time*, although the static averages turn out to be the same. An alternative approach to the investigation of time dependent properties is to generate initial states, drawn from a canonical ensemble using Monte Carlo methods, and to use these as starting points for the integration of the coupled equations of motion. This method has been around for some three decades, but it is only in recent years that efficient algorithms have been developed and computers have become sufficiently fast that it has become possible to garner substantial information about dynamic properties in 'interesting' regimes, e.g., near phase transitions.

The purpose of this article is to provide background on the spin dynamics method and to describe the current status of results. An important issue which will also be considered is the comparison between spin dynamics results and those of experiment on real, physical systems as well as with theory. For simplicity, we shall restrict ourselves to systems of $N$ fixed length, three-component, classical spins which interact with the general Hamiltonian

$$\mathcal{H} = -J \sum_{\langle i,j \rangle} (S_{ix} S_{jx} + S_{iy} S_{jy} + \lambda S_{iz} S_{jz}) + D \sum_i S_{iz}^2 + H \sum_i S_{iz} \tag{1.1}$$

where the first sum is over all nearest neighbour pairs, $\lambda$ represents exchange anisotropy, $D$ is the single ion anisotropy and $H$ is the external magnetic field. There are a number of physical systems which are well approximated by (1.1), although for different systems, and different experimental conditions one or more of the parameters may vanish. For $\lambda = 1$ and

0953-8984/99/180179+35$19.50  

$D = 0$ (1.1) represents the classical, isotropic Heisenberg ferromagnet or the corresponding antiferromagnet for $J > 0$ or $J < 0$, respectively. Research in the general area of critical dynamics is now quite widespread and in the space available here it is simply not possible to review all relevant material. We, therefore, emphasize at the outset that we have made a subjective choice of the topics to be reviewed here and apologize in advance to those authors whose work is not cited here.

## 2. Theoretical background

### *2.1. Critical dynamics in magnets*

The dynamic properties of magnetic systems have been of great theoretical interest for over 30 years. The behaviour of propagating modes, such as spin waves, at low temperatures and spin diffusion at high temperatures has been studied extensively. One particularly intriguing aspect of the time dependent behaviour of magnetic systems is the 'critical slowing down' which occurs as a second-order phase transition is approached. In a classic exposition, Hohenberg and Halperin (1977) described the framework for understanding dynamic critical behaviour in terms of universality classes which depended on a small number of properties of the models such as lattice dimensionality $d$ and symmetry of the Hamiltonian. A new dynamic critical exponent $z$ was introduced to describe the divergence of the characteristic times scale as the critical point is approached. Explicit predictions were made for simple models such as the isotropic Heisenberg ferromagnet and antiferromagnet in $d = 3$. In the following discussion we confine ourselves to systems with short range interactions; the modifications which are necessary when dipolar couplings are present have been reviewed by Frey and Schwabl (1994) and will be treated only briefly here.

At the critical point $T_c$ of an infinite system, the correlation time $\tau$ grows as $\tau \sim |\boldsymbol{q}|^{-z}$ as the wave vector $\boldsymbol{q}$ of the mode approaches zero. Associated with the time scale $\tau$ there is a characteristic frequency $\omega$ which has the scaling form

$$\omega = |\boldsymbol{q}|^{z}\Omega(|\boldsymbol{q}||T - T_c|^{-\nu}) \tag{2.1}$$

where $\nu$ is the critical exponent of the correlation length. If the system is confined to a finite box $L^d$ the relaxation time of the $\boldsymbol{q} = \boldsymbol{0}$ mode grows as $\tau \sim L^z$ at $T = T_c$, a behaviour which can be justified within the framework of dynamic finite-size scaling described in section 5.

The analytical theory of critical dynamics in classical Heisenberg ferro- and antiferromagnets in $d > 2$ is based on the Ginzburg–Landau Hamiltonian

$$\mathcal{H}_{GL} = \int \mathrm{d}^d x \left[\frac{1}{2}|\nabla\Phi|^2 + \frac{r}{2}|\Phi|^2 + u|\Phi|^4\right] \tag{2.2}$$

for a three-component order parameter $\Phi$, where $r \propto (T - T_c)/T_c$ is a measure of the reduced temperature and $u$ is the coupling constant. The static critical behaviour of Heisenberg ferro- and antiferromagnets in $2 < d \leqslant 4$ is captured by (2.2). Within this coarse grained picture the dynamics of an isotropic ferromagnet, which has been classified as model J by Hohenberg and Halperin (1977), can be written in the form of the Langevin equation

$$\begin{aligned} \frac{\partial\Phi}{\partial t} &= \lambda_0\nabla^2\frac{\delta\mathcal{H}}{\delta\Phi} + g_0\Phi \times \frac{\partial\mathcal{H}}{\partial\Phi} + \Theta \\ \mathcal{H} &= \mathcal{H}_{GL} - \int \mathrm{d}^d\Phi \cdot \boldsymbol{h}(\boldsymbol{x}, t) \end{aligned} \tag{2.3}$$

where the magnetization (order parameter) $\Phi$ is conserved and $\Theta = (\theta_1, \theta_2, \theta_3)$ denotes a Gaussian distributed white noise source with zero mean and correlations according to

$$\langle\theta_\alpha(x, t)\theta_\beta(x', t')\rangle = -2\lambda_0\nabla^2\delta(x - x')\delta(t - t')\delta_{\alpha,\beta}. \tag{2.4}$$

$\lambda_0$ and $g_0$ are Onsager coefficients. Note that (2.4) ensures the validity of the dissipation–fluctuation theorem. The dynamic exponent $z$ for model J is given by

$$z = \frac{1}{2}(d + 2 - \eta) = d - \frac{\beta}{\nu}. \tag{2.5}$$

A simple argument which leads to (2.5) can be obtained from the behaviour of (2.3) for $T > T_c$: the only remaining characteristic frequency, the Larmor frequency, is proportional to a magnetic field and thus has the same scaling dimension (Wagner 1970, Bausch *et al* 1976).

For an isotropic antiferromagnet the dynamics is quite different although the static critical behaviour is still described by (2.2). In contrast to the ferromagnetic case, the order parameter $\Phi$ (staggered magnetization) is no longer conserved. Furthermore, the time evolution of the order parameter is coupled to the usual magnetization $\boldsymbol{m}$ whose magnitude is a *conserved* quantity that does not affect the static critical behaviour. The Langevin equations for the isotropic antiferromagnet are classified as model G (Hohenberg and Halperin 1977):

$$\begin{aligned}
&\frac{\partial \Phi}{\partial t} = -\Gamma_0 \frac{\delta \mathcal{H}}{\delta \Phi} + g_0 \Phi \times \frac{\delta \mathcal{H}}{\delta \boldsymbol{m}} + \Theta \\
&\frac{\partial \boldsymbol{m}}{\partial t} = \lambda_0 \nabla^2 \frac{\delta \mathcal{H}}{\delta \boldsymbol{m}} + g_0 \Phi \times \frac{\delta \mathcal{H}}{\delta \Phi} + g_0 \boldsymbol{m} \times \frac{\delta \mathcal{H}}{\delta \boldsymbol{m}} + \Xi \\
&\mathcal{H} = \mathcal{H}_{GL} + \int \mathrm{d}^d x \frac{|m|^2}{2\chi_m} - \int \mathrm{d}^d x (\Phi \cdot \boldsymbol{h}(\boldsymbol{x}, t) + \boldsymbol{m} \cdot \boldsymbol{h}_m(\boldsymbol{x}, t)).
\end{aligned} \tag{2.6}$$

The noise sources $\Theta = (\theta_1, \theta_2, \theta_3)$ and $\Xi = (\zeta_1, \zeta_2, \zeta_3)$ are again Gaussian with zero mean, but

$$\langle \theta_\alpha(\boldsymbol{x}, t) \theta_\beta(\boldsymbol{x}', t') \rangle = 2\Gamma_0 \delta(\boldsymbol{x} - \boldsymbol{x}') \delta(t - t') \delta_{\alpha,\beta} \tag{2.7}$$

where the correlations of $\Xi$ are given by (2.4). Note that the order parameter $\Phi$ and the magnetization are not coupled by the Hamiltonian $\mathcal{H}$. In contrast to the ferromagnet the spin wave spectrum for the antiferromagnet is *linear* in $\boldsymbol{q}$ for small $|\boldsymbol{q}|$

$$\omega(\boldsymbol{q}) = c_s |\boldsymbol{q}| \text{ with } c_s^2 = \rho_s / \chi_m \tag{2.8}$$

where $c_s$ is the spin wave velocity. The susceptibility $\chi_m$ is always finite, whereas the stiffness constant (helicity modulus) $\rho_s$ exhibits a critical singularity at the Néel temperature $T_N$, i.e. $\rho_s \sim (T_N - T)^{\nu(d-2)}$ for $T \leqslant T_N$. In order to reconcile (2.8) with the general scaling form given by (2.1) for $T_c = T_N$ one has to set $\Omega(x) \sim x^{1-z}$ for $x \ll 1$, i.e. for $T < T_N$ and $\boldsymbol{q} \to \boldsymbol{0}$. From the temperature singularity of $c_s$ one obtains

$$z = d/2. \tag{2.9}$$

Another interesting case is provided by *anisotropic* Heisenberg ferromagnets (see (1.1) for $\lambda \neq 1$). In contrast to the dynamics in an isotropic ferromagnet only the $z$ component of the magnetization is still conserved. For $\lambda = 0$ (1.1) describes a planar ferromagnet, which has the same static critical behaviour as an $XY$ model. According to the modified conservation laws the dynamics of the planar ferromagnet represents a universality class distinct from the ones mentioned above and has been classified as model E (Hohenberg and Halperin 1977). In terms of a complex order parameter $\Phi \equiv m_x + \mathrm{i}m_y$ and the conserved $z$ component $m \equiv m_z$ of the magnetization the Langevin equations read

$$\begin{aligned}
&\frac{\partial \Phi}{\partial t} = -\Gamma_0 \frac{\delta \mathcal{H}}{\delta \Phi *} - \mathrm{i} g_0 \Phi \frac{\delta \mathcal{H}}{\delta \boldsymbol{m}} + \Theta \\
&\frac{\partial m}{\partial t} = \lambda_0 \nabla^2 \frac{\delta \mathcal{H}}{\delta m} + 2 g_0 \mathrm{Im} \left( \Phi * \frac{\delta \mathcal{H}}{\delta \Phi *} \right) + \zeta \\
&\mathcal{H} = \mathcal{H}_{GL} + \int \mathrm{d}^d x \frac{m^2}{2C_0} - \int \mathrm{d}^d x (\mathrm{Re}\,(\Phi * h(\boldsymbol{x}, t)) + m h_m(\boldsymbol{x}, t))
\end{aligned} \tag{2.10}$$

where $\Theta = \theta_x + \mathrm{i}\theta_y$ and $\zeta$ are noise sources according to (2.7) and (2.4), respectively. If (2.10) is rewritten in components $(m_x, m_y, m_z)$ of the magnetization, one immediately recovers the components of the usual Larmor term for the planar ferromagnet. By inspection of equation (2.10) one obtains the impression that the dynamics of a planar ferromagnet is closer to the dynamics of the isotropic *antiferromagnet* (model G) than to the dynamics of the isotropic ferromagnet (model J). This is indeed the case even in a quantitative sense, because the dynamic exponent $z$ is found to be the same as for model G (see (2.9)) by virtue of the same arguments (Hohenberg and Halperin 1977).

### *2.2. Mode coupling theory of spin dynamics*

Another theoretical approach to the dynamics of magnetic systems which is also based on a coarse grained picture of magnets is provided by mode-coupling theory (see Kawasaki (1976) for an extended review of this technique). As a starting point one considers the Heisenberg equations of motion for the spin operators $S_q^\alpha(t)$ in momentum space. For, e.g., an isotropic Heisenberg model for $\lambda = 1$ and $D = 0$, one obtains in $d = 3$ ($\hbar = 1$)

$$\begin{aligned} \frac{\mathrm{d}}{\mathrm{d}t} S_q^z &= -\mathrm{i} \int \frac{\mathrm{d}^3 k}{(2\pi)^3} (J(\boldsymbol{k}) - J(\boldsymbol{q}-\boldsymbol{k})) S_{q-k}^+ S_k^- \\ \frac{\mathrm{d}}{\mathrm{d}t} S_q^\pm &= \pm 2\mathrm{i} \int \frac{\mathrm{d}^3 k}{(2\pi)^3} (J(\boldsymbol{k}) - J(\boldsymbol{q}-\boldsymbol{k})) S_{q-k}^\pm S_k^z \end{aligned} \tag{2.11}$$

where $S_q^\pm = S_q^x \pm \mathrm{i} S_q^y$ are the ladder spin operators and $J(\boldsymbol{q}) = -J_0 + J_1 \boldsymbol{q}^2 + \cdots$ is the Fourier transform of the exchange coupling expanded for small momenta $\boldsymbol{q}$. From (2.11) one obtains the mode coupling equations for correlation functions on a coarse grained timescale by a projection on slow variables like the order parameter or the energy density. For the systems discussed here the quantities of main interest are the Kubo relaxation functions which are defined by (Thoma *et al* 1991)

$$\phi^{\alpha,\beta}(\boldsymbol{q}, t) = \mathrm{i} \lim_{\varepsilon \to 0} \int_t^\infty \mathrm{d}\tau \mathrm{e}^{-\varepsilon\tau} \langle [X_q^\alpha(\tau), X_q^\beta(0)^+] \rangle \tag{2.12}$$

where $X_q^\alpha(t) \equiv S_q^\alpha(t)/\sqrt{\chi^\alpha(\boldsymbol{q})}$ are normalized spin variables and the $\chi^\alpha(\boldsymbol{q})$ are the static spin–spin correlation functions. The equation of motion for $\phi^{\alpha,\beta}$ then reads

$$\frac{\partial}{\partial t} \phi^{\alpha,\beta}(\boldsymbol{q}, t) = \mathrm{i}\omega^{\alpha,\gamma}(\boldsymbol{q}) \phi^{\gamma,\beta}(\boldsymbol{q}, t) - \int_0^t \mathrm{d}\tau \Gamma^{\alpha\gamma}(\boldsymbol{q}, t-\tau) \phi^{\gamma,\beta}(\boldsymbol{q}, \tau) \tag{2.13}$$

where $\omega^{\alpha,\beta}(\boldsymbol{q}) = -\langle [X_q^\alpha(0), X_{-q}^\beta(0)] \rangle$ is the frequency matrix which contains all *linear* contributions to spin dynamics and relaxation. The nonlinearities are captured by the memory kernel $\Gamma^{\alpha,\beta}(\boldsymbol{q}, t)$ which depends on higher correlation functions between the spin variables. If, e.g., only two-mode processes are retained, $\Gamma^{\alpha,\beta}(\boldsymbol{q}, t)$ becomes bilinear in $\phi^{\alpha,\beta}(\boldsymbol{q}, t)$. With this approximation mode coupling theory for the isotropic ferromagnet is consistent with dynamic scaling in the critical regime, where $z = (5 + \eta)/2$ is obtained in $d = 3$, a result which is at variance with (2.5). In order to reproduce (2.5) higher order and vertex corrections must be taken into account (Frey and Schwabl 1994). For the isotropic antiferromagnet (Kawasaki 1976) and the planar ferromagnet (Thoma *et al* 1991) dynamic scaling is obtained with the correct value $z = 3/2$ of the dynamic exponent within the two-mode approximation for the memory kernel in $d = 3$. If (2.13) is Fourier transformed into frequency space, a set of self-consistent integral equations for $\phi^{\alpha,\beta}(\boldsymbol{q}, \omega)$ is obtained. For many practical purposes the frequency dependence of $\Gamma^{\alpha,\beta}(\boldsymbol{q}, \omega)$ is weak so that these functions can be replaced by their value at $\omega = 0$. In this case the Kubo relaxation functions (line shapes) become Lorentzian in $\omega$ (Thoma *et al* 1991, Frey and Schwabl 1994).

Mode coupling theory has also been applied in $d = 3$ to ferromagnets with dipolar interactions (Frey and Schwabl 1994), which due to their long ranged nature are expected to dominate the critical behaviour. Furthermore, dipolar forces are anisotropic and therefore the magnetization in ferromagnets is no longer a conserved quantity. If exchange interactions are also present, a new length scale $1/q_D$ emerges which keeps the longitudinal component of the static susceptibility finite at $T_c$, whereas the transverse component diverges. Accordingly, dynamic scaling differs for longitudinal and transverse modes and the scaling functions depend on the dimensionless ratio $|\boldsymbol{q}|/q_D$. For longitudinal modes, $z_\parallel = 0$ in the dipolar regime, i.e., the characteristic frequency remains *finite* at $T = T_c$ for $\boldsymbol{q} \to \boldsymbol{0}$. For transverse modes, $z_\perp = 2$, which is the classical value for purely relaxational dynamics without conservation laws (model A of Hohenberg and Halperin (1977)). Within the same approximations one obtains $z = 5/2$ for the usual short-ranged exchange interactions. Note that $z = 5/2$ is consistent with (2.5) in $d = 3$ within the Ornstein–Zernicke approximation ($\eta = 0$). The crossover from isotropic ($z = 5/2$) to dipolar ($z_\parallel = 0$ and $z_\perp = 2$) critical behaviour, is entirely captured by the scaling functions of the characteristic frequencies and can be described within the Lorentzian approximation for the Kubo relaxation functions.

### *2.3. Magnetic chains in external fields: solitons*

There is a wide body of literature on the theory of magnetic systems in $d = 1$ spatial dimensions. We will therefore only focus on a particularly interesting set of questions which arises when one looks at ferromagnetic Heisenberg chains with a planar anisotropy in a symmetry breaking field. An effective continuum model for this problem turns out to be given by the classical sine–Gordon model (Mikeska 1978, Allroth and Mikeska 1981a, b). The elementary excitations consist of plane (spin) waves and solitons which in their simplest form may be visualized as localized $\pm 2\pi$ twists of spins along the chain. In the different components of the dynamic structure factor these excitations appear as central soliton peaks. A single spin-wave peak in $S_y^{SW}(q, \omega)$ is predicted to be a simple $\delta$ function

$$S_y^{SW}(q, \omega) = \frac{k_B T}{4\pi(m^2 + q^2)} \delta(\omega - \omega_q) \tag{2.14}$$

where $m$ is the soliton rest mass. With spin-wave interactions $S_y(q, \omega)$ becomes Lorentzian,

$$\delta(\omega - \omega_q) \to \frac{1}{\pi} \frac{\Gamma}{(\omega - \omega_q)^2 + \Gamma^2}. \tag{2.15}$$

The central soliton peak has a Gaussian line shape

$$S_\alpha^{sol}(q, \omega) = \left[1 - \frac{k_B T}{2m}\left[1 - \frac{m^2 + q^2}{12m^2}\right]\right] \frac{32}{cq\pi m^2} \left[\frac{m}{\pi k_B T}\right]^{1/2} n \exp\left[\frac{4m\omega^2}{k_B T c^2 q^2}\right] f_\alpha(q) \tag{2.16}$$

where $n$ is the soliton density, which increases as $\exp(-8m/k_B T)$, and $f_x(q)$ and $f_y(q)$ differ. There should be no single spin-wave peak in $S_{xx}(q, \omega)$ but rather a two-spin-wave signal with step-like and square-root singularities. In the sine–Gordon description the spins are confined to the $xy$ plane so that no predictions are made about $S_{zz}(q, \omega)$. The general picture given by the sine–Gordon theory has been confirmed by spin dynamics simulations of an $XY$ chain in a magnetic field (Gerling and Landau 1990), but the quantitative agreement with the theory remains unsatisfactory.

### *2.4. Two-dimensional easy plane magnets and the XY model*

The $d = 2$ $XY$ ferromagnet (anisotropic Heisenberg model) is one of the 'special' models of magnetism. It undergoes an unusual phase transition to a state with bound, topological

excitations (vortex pairs) but no long range order (Kosterlitz and Thouless 1973). The (three-component) $XY$ model may be viewed as a special case of the anisotropic Heisenberg model in which the coupling between the $z$ components of spins vanishes ((1.1) with $\lambda = 0$, $D = 0$). It has static properties which are similar to those of the 'plane rotator' model, in which the spins have only two components. The static behaviour of both models has been studied by simulation (see, e.g., Tobochnik and Chester 1979, Gerling and Landau 1984, Gupta and Baillie 1992, Janke and Nather 1993) and found to be consistent with the predictions of the Kosterlitz–Thouless theory. For example, the susceptibility shows an essential singularity instead of a power law divergence, and vortex pairs unbind at $T_{KT}$.

The $XY$ model has true dynamics which can be determined by integrating the equations of motion for each spin whereas the 'plane rotator' model has only stochastic, i.e. relaxational, time dependence which has been examined by Monte Carlo simulation (Gupta and Baillie 1992). Note that *different* dynamic exponents are expected for stochastic and for true dynamics (Hohenberg and Halperin 1977). $m_z$ is conserved during the time evolution; so that the out-of-plane component $S^{zz}$ and in-plane component $S^{xx} = S^{yy}$ can be separated. The dynamics of $d = 2$ systems with easy-plane asymmetry were first analysed by Villain (1974, 1975) and by Moussa and Villain (1976). $S^{xx}(q, \omega)$ was found to have a $\delta$ function spin-wave peak at low temperature and near $T_{KT}$ a spin-wave peak of the form

$$S^{xx}(q, \omega) \sim \frac{1}{|\omega - \omega_q|^{1-\eta/2}}. \tag{2.17}$$

Here $\omega_q$ is the position of the spin-wave peak and $\eta$ is the exponent describing the decay of the static spin–spin correlation function ($\eta = 1/4$ at $T_{KT}$). At high temperatures, Moussa and Villain (1976) predict that $S^{xx}(q, \omega)$ is given by the sum of two non-divergent terms.

In spatial dimensions $d \leqslant 2$ the description of the static behaviour of Heisenberg-like systems is no longer captured by the Ginzburg–Landau Hamiltonian given by (2.2). Instead, one can use an adapted version of the well known nonlinear sigma model, which in the case of a planar ferromagnet has been considered in the form (Nelson and Fisher 1977)

$$\mathcal{H} = \frac{1}{2} \int \mathrm{d}^d x [(\nabla m_x)^2 + (\nabla m_y)^2 + m_z^2] \tag{2.18}$$

with the constraint $m_x^2 + m_y^2 = 1$, neglecting coupling between $m_z$ and the other components of $\boldsymbol{m}$. They obtained the transverse spin–spin correlation function,

$$C^{xx}(r, t) \sim 1/r^\eta \, \Psi_\eta(ct/r) \tag{2.19}$$

$$\Psi_\eta(y) = \begin{cases} 1 & y < 1 \\ (y + \sqrt{y^2 - 1})^{-\eta} & y > 1 \end{cases}$$

where $c$ is the spin-wave velocity and $t$ is the time. The Fourier transform of (2.19) is

$$S^{xx}(q, \omega) \sim \frac{1}{q^{3-\eta}} \Psi\left(\frac{\omega}{cq}\right) \tag{2.20}$$

where the scaling function $\psi$ behaves like

$$\Psi(y) \sim \frac{1}{|1 - y^2|^{1-\eta}} \tag{2.21}$$

around the spin-wave peak, and

$$S^{xx}(q, \omega) \sim \omega^{\eta - 3} \qquad \omega \gg \omega_q. \tag{2.22}$$

They also predicted that the dynamic critical exponent, which should be $z = d/2$ for $d > 2$ (Hohenberg and Halperin 1977), is $z = 1$ for $d \leqslant 2$. Note that the value $z = 1$ and a

*linear* dispersion relation are also implicit in the argument of the scaling function $\Psi$ in (2.20). Finally, both theories predict a $\delta$ function spin-wave peak in $S^{zz}(q,\omega)$, at $\omega = cq$. More recently, Menezes *et al* (1993) performed a low temperature calculation which includes the out-of-plane fluctuations and found a similar spin-wave peak as Nelson and Fisher,

$$S^{xx}(q,\omega) \sim \eta^2 \frac{1}{q^3|\hat{\omega}||1-\hat{\omega}^2|} \tag{2.23}$$

plus a logarithmically divergent central peak

$$S^{xx}(q,\omega) \sim \eta^2 \frac{\log(1/\hat{\omega})}{q} \tag{2.24}$$

where $\hat{\omega} = \omega/(cq)$. Of course, a central peak at low temperature can also be caused by other mechanisms, e.g. vortex pairs diffusing like a dilute pair of solitons (Pereira *et al* 1992). Very narrow peaks are predicted for $S_{zz}(q,\omega)$ (Menezes *et al* 1992).

For a phase transition of Kosterlitz–Thouless type, the spin stiffness should drop discontinuously to zero at $T_{KT}$, i.e. the spin-wave peak is predicted to disappear (Nelson and Fisher 1977, Nelson and Kosterlitz 1977). Above $T_{KT}$, vortex–antivortex pairs unbind, and their diffusion leads to a strong central peak in $S(q,\omega)$. Mertens *et al* (1987, 1988) calculated $S(q,\omega)$ above $T_{KT}$, assuming an ideal dilute gas of unbound vortices moving in the presence of renormalized spin waves and screened by the remaining vortex–antivortex pairs. They find a Lorentzian central peak for $S^{xx}(q,\omega)$,

$$S^{xx}(q,\omega) \sim \frac{\gamma^3\xi^2}{[\omega^2+\gamma^2[1+(\xi q)^2]]^2} \tag{2.25}$$

and a Gaussian central peak for $S^{zz}(q,\omega)$,

$$S^{zz}(q,\omega) \sim \frac{n_v\bar{u}}{q^3}\exp\left\{-\left(\frac{\omega}{\bar{u}q}\right)^2\right\} \tag{2.26}$$

where $\gamma = (\sqrt{\pi}/2)\bar{u}/\xi$, $\bar{u}$ is the rms vortex velocity and $n_v \sim (2\xi)^{-2}$ the free vortex density.

Early analytical work on vortex dynamics in 2D Heisenberg ferromagnets with a planar anisotropy (see (1.1) with $0 < \lambda < 1$ and $D = 0$) focused on vortex motion in a diluted vortex gas for $T > T_{KT}$ (Huber 1978). The vortex contribution to the in-plane spin autocorrelation function shows a vanishing decay rate at $T \to T_{KT}$ due to the disappearance of free vortices. However, the faster decay of multiple spin-wave contribution obscures the critical slowing down. In the out-of-plane component, vortices lead to a narrow central peak on top of a broad spin-wave background. The quantitative picture of the critical dynamics is expected to hold for all $q$ values outside the hydrodynamic regime. More recently, additional vortex dynamics calculations have been performed for easy-plane Heisenberg ferromagnets (Mertens *et al* 1988, 1989, Gouvêa *et al* 1989) and their antiferromagnetic counterparts (Völkel *et al* 1991a, b). Above $T_{KT}$, $S_{xx}(\boldsymbol{q},\omega)$ is given by a squared Lorentzian, whereas $S_{zz}(\boldsymbol{q},\omega)$ displays a Gaussian shape where the line widths depend on the root-mean-square vortex velocity. Note that for both ferro- and antiferromagnets planar vortices should only be stable for values $\lambda < \lambda_c$; above $\lambda_c$ the vortices develop an out-of-plane component with a bell-shape distribution centred at the vortex core.

## 3. Experimental background

Experimental investigation of dynamics in magnetic systems can be effectively studied using inelastic neutron scattering techniques. These experiments measure the dynamic structure factor, $S(q,\omega)$, the properties of which yield information about elementary excitations and

dynamic critical behaviour. These experiments are more difficult than elastic scattering studies because of the greatly reduced signal to noise ratio. Typically critical properties are examined by measuring various intensities and lineshapes as a function of the reduced distance from the critical point $T_c$. In the case of dynamic critical behaviour this means measuring the $\boldsymbol{q}$ dependence of the dynamic response at $T_c$ for $\boldsymbol{q} \to \boldsymbol{0}$. This means, of course, that the critical temperature must be accurately known and the dynamic structure factor for small $\boldsymbol{q}$ and the resolution function must be accurately determined. Another difficulty which is faced in carrying out experimental studies is that of finding physical systems which can be well approximated by the simple magnetic models discussed above. Fortunately, there are several well studied systems which can be described by simple Hamiltonians of the kind in equation (1.1). Examples include $CsNiF_3$ as a prototype of a 1D soliton bearing system, $CoCl_2$-GIC as an example of a 2D $XY$ system, and EuS and $RbMnF_3$ as examples of an isotropic 3D Heisenberg ferromagnet and antiferromagnet respectively. Lastly, anisotropic 3D systems are well represented by $MnF_2$ and $FeF_2$. Some of these experimental results will be described later.

## 4. Spin dynamics methods

### *4.1. Equations of motion*

For models with continuous degrees of freedom, real equations of motion,

$$\frac{\mathrm{d}\boldsymbol{S}_i}{\mathrm{d}t} = \frac{\partial \mathcal{H}}{\partial \boldsymbol{S}_i} \times \boldsymbol{S}_i = -\boldsymbol{S}_i \times \boldsymbol{H}_{eff} \tag{4.1}$$

describe the dynamics where $\boldsymbol{H}_{eff}$ is an 'effective' interaction field. For the isotropic Heisenberg ferromagnet $\boldsymbol{H}_{eff} = -J \sum_{nn} \boldsymbol{S}_j$ and the time dependence of each spin, $\boldsymbol{S}_r(t)$, can be determined from integration of these equations (Gerling and Landau 1984). These coupled equations of motion can be viewed as describing the precession of each spin about an effective interaction field; the complexity arises from the fact that, since all spins are moving, the effective field is not static but rather itself constantly changing direction and magnitude.

### *4.2. Time integration algorithms*

A number of algorithms are available for the integrations of the coupled equations of motion which were derived in the previous sub-section. The simplest approach is to simply expand about the current spin value using the time-step $\Delta$ as the expansion variable;

$$S_i^\alpha(t+\Delta) = S_i^\alpha(t) + \Delta S_i^\alpha(t) + \frac{1}{2}\Delta^2 \ddot{S}_i^\alpha(t) + \frac{1}{3!}\Delta^3 \dddot{S}_i^\alpha(t) + \cdots \tag{4.2}$$

where the $\alpha$ denotes the spin component. The 'new' estimate may be made by simply evaluating as many terms as possible in the sum, although this procedure must obviously be truncated at some point. Of course, values of the various time derivatives must be obtained and, except for $\dot{S}_i^\alpha$ which can be obtained directly from (1.1), these calculations may be somewhat time consuming. Typical values of $\Delta$ which deliver reliable results to a reasonable maximum integration time $t_{max}$ are in the range of $\Delta = 0.005$. If the equation is truncated at the point shown in (4.3), the errors will be of order $\Delta^4$. A very simple improvement can be made by implementing a 'leapfrog' procedure in which one also expands using $-\Delta$ as the expansion variable and subtracts the resulting equation from (4.2) to yield

$$S_i^\alpha(t+\Delta) = S_i^\alpha(t-\Delta) + 2\Delta \dot{S}_i^\alpha(t) + \frac{2}{3!}\Delta^3 \dddot{S}_i^\alpha(t) + \cdots. \tag{4.3}$$

The error in this integration is $\mathcal{O}(\Delta^5)$ and allows not only larger values of $\Delta$ to be used but also allows us to extend the maximum integration time to $t_{max} \approx 100J^{-1}$. Several standard numerical methods can also be applied. One excellent approach is to use a predictor–corrector method; fourth-order predictor–corrector methods have proven to be quite effective. An example is the explicit four-step Adams–Bashforth method (Burden *et al* 1981)

$$S_i^\alpha(t+\Delta) = S_i^\alpha(t) + \tfrac{1}{24}\Delta[55S_i^\alpha(t) - 59S_i^\alpha(t-\Delta) + 37S_i^\alpha(t-2\Delta) - 9S_i^\alpha(t-3\Delta)] \tag{4.4}$$

followed by an implicit Adams–Moulton corrector step

$$S_i^\alpha(t+\Delta) = S_i^\alpha(t) + \tfrac{1}{24}\Delta[9S_i^\alpha(t+\Delta) + 19S_i^\alpha(t) - 5S_i^\alpha(t-\Delta) + S_i^\alpha(t-2\Delta)] \tag{4.5}$$

a combination which also has a local truncation error of $\Delta^5$ and which has proven to be quite successful. The first application of (4.4) obviously requires that at least three time steps have already been taken; these can initially be provided using the fourth-order Runge–Kutta method, starting with the initial state. Of course, this predictor–corrector method requires that the spin configuration at four time steps must be kept in memory. Note that the conservation laws discussed earlier will only be observed within the accuracy set by the truncation error of the method. In practice, this limits the time step to typically $\Delta = 0.01/J$ in $d = 3$ (Chen and Landau 1994) for the isotropic model ($D = 0$), where $t_{max} \leqslant 200/J$. The same method was used in $d = 2$; with a time step $\Delta = 0.025/J$ (Costa *et al* 1997), $t_{max} \leqslant 60/J$, whereas with $\Delta = 0.01/J$, $t_{max} = 400/J$ (Evertz and Landau 1996) could be achieved.

For a typical spin dynamics study the major part of the CPU time needed is consumed by the numerical time integration. The biggest possible time step is thus most desirable; however, 'standard' methods impose a severe restriction on the size of $\Delta$ for which the conservation laws of the dynamics are obeyed. It is evident from (4.1) that $|\boldsymbol{S}_i|$ for each lattice site $i$ and the total energy are conserved. Symmetries of the Hamiltonian impose additional conservation laws, so, e.g. for $D = 0$ and $\lambda = 1$ (isotropic Heisenberg model) the magnetization $\boldsymbol{m}$ is conserved. For an anisotropic Heisenberg model, i.e., $\lambda \neq 1$ or $D \neq 0$, only the $z$ component $m_z$ of the magnetization is conserved. Conservation of spin length and energy is particularly crucial, and it would therefore also be desirable to devise an algorithm which conserves these two quantities exactly. Thus, a new, large time step integration procedure, which is based on Trotter–Suzuki decompositions of exponential operators and conserves both spin length and energy *exactly* for $D = 0$, has been devised. The motion of a spin, given by (4.1), may be visualized as a precession of the spin $\boldsymbol{S}_i$ around an effective field $\boldsymbol{H}_{eff}$ which is itself time dependent. For the simple case $D = 0$, and arbitrary values of $\lambda$, the lattice can be decomposed into two sublattices such that a spin on one sublattice performs a precession in a local field $\boldsymbol{H}_{eff}$ of neighbour spins which are *all* located on the other sublattice. First, each spin on a sublattice is rotated about its local field $\boldsymbol{H}_{eff}$ by an angle $\alpha = |\boldsymbol{H}_{eff}|\Delta$, guaranteeing conservation of the spin length to within machine accuracy, and the process is then carried out for spins on the other sublattice. The sublattice equations of motion reduce to a linear system of differential equations if the spins on the other sublattice are kept fixed, so an alternating update scheme is used. Note, that each sublattice rotation is performed with the current values of the spins on the other sublattice, so that only a single copy of the spin configuration is kept in memory at any time. However, the magnetization will not be conserved during the above rotation operations; moreover, the two alternating rotation operations do not commute, so that a closer examination of the sublattice decomposition of the spin rotation is required. The cross products in the equations of motion can expressed by matrices **A** and **B** which are the generators of the rotation of the spin configuration $\boldsymbol{S}_{i\mathcal{A}}$ on sublattice $\mathcal{A}$ at fixed $\boldsymbol{S}_{i\mathcal{B}}$ and of the spin configuration $\boldsymbol{S}_{i\mathcal{B}}$ on sublattice $\mathcal{B}$ at fixed $\boldsymbol{S}_{i\mathcal{A}}$, respectively. The update of the configuration can then be expressed by an exponential (matrix) operator by

$$\boldsymbol{S}_i(t+\Delta) = \mathrm{e}^{(\mathbf{A}+\mathbf{B})\Delta}\boldsymbol{S}_i(t). \tag{4.6}$$

Although the exponential operator has no simple explicit form, because the rotation axis for each spin depends on the configuration itself and is therefore not known *a priori*, the operators $e^{\mathbf{A}\Delta}$ and $e^{\mathbf{B}\Delta}$ do have a simple explicit form. The alternating update amounts to the replacement of $e^{(\mathbf{A}+\mathbf{B})\Delta}$ by $e^{\mathbf{A}\Delta}\,e^{\mathbf{B}\Delta}$ which is only correct up to terms of the order $\Delta^2$ (Suzuki and Umeno 1993). The magnetization will thus only be conserved up to terms of the order $\Delta$, but further improvement is possible by employing higher order Suzuki–Trotter decompositions of the exponential to decrease the local truncation error, e.g. to second order:

$$e^{(\mathbf{A}+\mathbf{B})\Delta} = e^{\mathbf{A}\Delta/2}\,e^{\mathbf{B}\Delta}\,e^{\mathbf{A}\Delta/2} + \mathcal{O}(\Delta^3) \tag{4.7}$$

which is equivalent to the midpoint integration method applied to (4.6) and to fourth order:

$$e^{(\mathbf{A}+\mathbf{B})\Delta} = \prod_{i=1}^{5} e^{p_i\mathbf{A}\Delta/2} e^{p_i\mathbf{B}\Delta} e^{p_i\mathbf{A}\Delta/2} + \mathcal{O}(\Delta^5) \tag{4.8}$$

with the parameters $p_1 = p_2 = p_4 = p_5 \equiv p = 1/(4-4^{1/3})$, and $p_3 = 1-4p$. The additional computational effort invested in the evaluation of (4.8) can be compensated by using larger time steps. (Note that the above decompositions maintain time reversal symmetry.) More distant neighbour two-spin interactions can be included if the lattice is decomposed into more sublattices, and the method can be generalized to the case $D \neq 0$ (Krech *et al* 1998).

A quantitative comparison of these integration methods was made for the simple cubic Heisenberg model with $\lambda = 1$ and $L = 10$. The same initial configurations were chosen by Monte Carlo simulation at $T = 0.8T_c$, where $T_c$ is the critical temperature of the isotropic model ($D = 0$). The equations of motion were integrated to $t_{max} = 800/J$ with $\Delta = 0.01/J$ for the predictor–corrector method in all cases. For $D = 0$ the energy per spin $e(t)$ for the predictor–corrector method increases linearly with time whereas the decomposition methods both yield $e(t) =$ const. The predictor–corrector method conserves $m(t)$ exactly, whereas the second-order decomposition with $\Delta = 0.04/J$ has fluctuations of $m(t)$ on all time scales, including $t > t_{max}$; the fourth-order decomposition method with $\Delta = 0.2/J$ gives remarkably good magnetization conservation despite the large time step. In order to achieve the same overall accuracy of the magnetization conservation with the second-order decomposition a time step $\Delta < 0.02/J$ is necessary. Both decomposition methods yield almost a net tenfold speedup over the predictor–corrector method.

For the strongly anisotropic case with $D = J$, the decomposition scheme must be modified because the spin rotation axis depends on the spin value at the future time $(t+\Delta)$ and an iterative solution is required. Even so, a 30% gain in speed remains. All three methods show a linear change in energy with time; a direct comparison of all three methods is displayed in figure 1. The overall accuracy of the magnetization conservation appears to be independent of $D$ for both decomposition methods. Considering both speed and overall energy conservation, the second-order decomposition has some advantages over the predictor–corrector method; if the emphasis is on energy conservation alone, the fourth-order method is best but only slightly faster. A direct comparison of $S(q, \omega)$ for the isotropic Heisenberg ferromagnet showed very good agreement between the results for the predictor–corrector method with $\Delta = 0.01/J$ and for the second-order decomposition method with $\Delta = 0.04/J$.

The great advantage of the predictor–corrector method is its versatility and its ability to conserve the magnetization exactly. Isotropic and anisotropic spin systems can be treated within the same numerical approach. The division of the lattice into sublattices, which is the basis for the decomposition method, depends on the range of the interactions, so that this approach is less general. Single-ion anisotropies leave the performance of the predictor–corrector method almost unaffected, whereas the decomposition method suffers from a drastic reduction in speed. The greatest advantage of the decomposition method is its capability

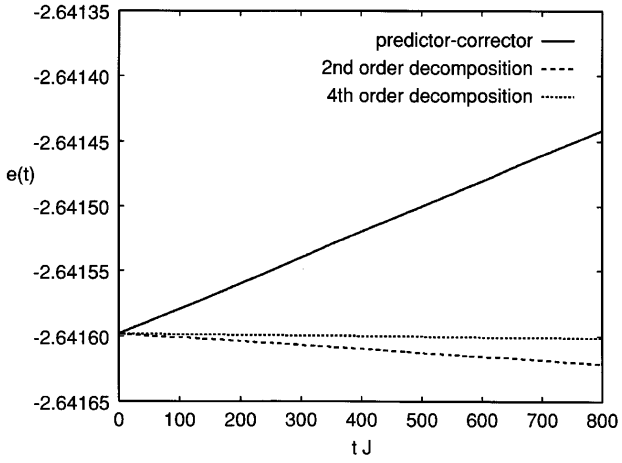


(*a*)

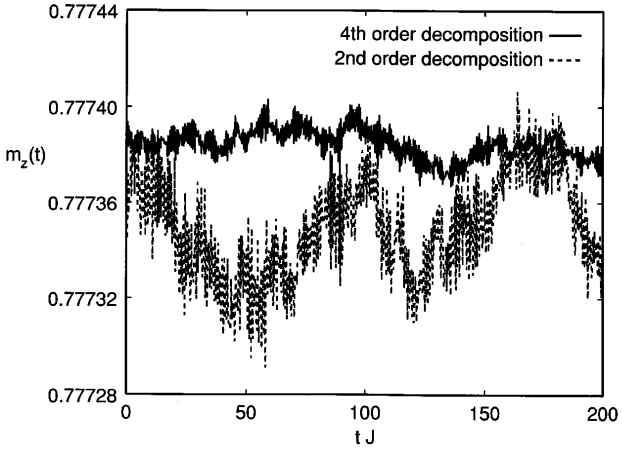


(*b*)

**Figure 1.** Spin dynamics data for the $L = 10$ simple cubic Heisenberg model with $D = J$. For the predictor–corrector method $\Delta = 0.01/J$, for the second-order decomposition method $\Delta = 0.04/J$ and for the fourth-order decomposition method $\Delta = 0.2/J$. (*a*) time dependence of the internal energy; (*b*) time dependence of the $z$ component of the magnetization. (From Krech *et al* 1998).

for handling large time steps and the exact conservation of spin length. In the absence of anisotropies it also conserves the energy exactly and maintains reversibility. For anisotropic Hamiltonians, energy conservation and reversibility can be obtained to a high accuracy using iterative schemes; but exact magnetization conservation is lost (figure 1).

### *4.3. Time-displaced correlation functions and Fourier transforms*

The space-displaced, time-displaced spin correlation function and its space–time Fourier transform are fundamental in the study of critical spin dynamics (Lovesey 1984). The correlation function is defined, with $k = x$, $y$ or $z$, as

$$C^k(\boldsymbol{r} - \boldsymbol{r}', t) = \langle S_r^k(t) S_{r'}^k(0)t\rangle - \langle S_r^k(t)\rangle\langle S_{r'}^k(0)\rangle \tag{4.9}$$

where $\langle \ldots \rangle$ denotes the ensemble average and the second term on the right-hand side should be constant, independent of position and time. The dynamic structure factor is given by

$$S^k(\boldsymbol{q},\omega) = \frac{1}{2\pi}\sum_{\boldsymbol{r},\boldsymbol{r}'} \mathrm{e}^{\mathrm{i}\boldsymbol{q}\cdot(\boldsymbol{r}-\boldsymbol{r}')}\int_{-\infty}^{\infty}\mathrm{e}^{\mathrm{i}\omega t}C^k(\boldsymbol{r}-\boldsymbol{r}',t)\,\mathrm{d}t \tag{4.10}$$

$S_k(\boldsymbol{q},\ \omega)$ is an experimental observable, for momentum transfer $\boldsymbol{q}$ and frequency $\omega$, in neutron scattering experiments. In practice, however, the time integration can only be carried out to some finite time cutoff which can introduce many oscillations into the result of the Fourier transform, (4.10). These oscillations, however, can be smoothed out by convoluting the spin correlation function with a resolution function in frequency (Gerling and Landau 1984) which plays the same role as does finite collimation in an experiment, i.e.,

$$\bar{S}^k(\bar{\boldsymbol{q}},\omega) = \frac{1}{2\pi}\sum_{\boldsymbol{r},\boldsymbol{r}'} \mathrm{e}^{\mathrm{i}\bar{\boldsymbol{q}}\cdot(\bar{\boldsymbol{r}}-\bar{\boldsymbol{r}}')}\int_{-t_{cutoff}}^{t_{cutoff}}\mathrm{e}^{\mathrm{i}\omega t}C^{\kappa}(\bar{\boldsymbol{r}}-\bar{\boldsymbol{r}}',t)\,\mathrm{e}^{-\frac{1}{2}(t\delta_\omega)^2}\mathrm{d}t \tag{4.11}$$

where $\delta_\omega$ is a parameter determining the resolution in frequency and needs to be chosen properly such that effects of the cutoff in the evolution time can be neglected.

### *4.4. Methods of analysis*

*4.4.1. Dynamic scaling.* The dynamic structure factor depends on the correlation length $\xi$ and may be written

$$S^k(\boldsymbol{q},\omega) = (2\pi/\omega_m)S^k(\boldsymbol{q})f(\omega/\omega_m,\boldsymbol{q},\xi) \tag{4.12}$$

where $\omega_m(\boldsymbol{q},\xi)$ is a 'characteristic frequency', $S^k(q) = \frac{1}{2\pi}\int_{-\infty}^{\infty}S^k(\bar{q},\omega)\mathrm{d}\omega$ and $f$ is a shape function satisfying the normalization condition (Halperin and Hohenberg 1967, Ferrell *et al* 1967). The characteristic frequency $\omega_m$ is a median frequency determined by the constraint

$$\int_{-\omega_m}^{\omega_m} S(\bar{q},\omega)\mathrm{d}\omega = \tfrac{1}{2}\int_{-\infty}^{\infty}S(\bar{q},\omega)\mathrm{d}\omega. \tag{4.13}$$

Dynamic scaling theory assumes that $\omega_m(\boldsymbol{q},\xi)$ is a homogeneous function of $q$ and $\xi$, i.e.

$$\omega_m = q^z\,\Omega(q\xi) \tag{4.14}$$

where $z$ is the dynamic critical exponent. Therefore $S^k_\xi(\boldsymbol{q},\omega)$ simplifies to

$$S^k(\boldsymbol{q},\omega) = (2\pi/\omega_m)S^k(\boldsymbol{q})f(\omega/\omega_m,\boldsymbol{q}\xi) \tag{4.15}$$

where the function $f$ depends only on the product of $q\xi$ but not on $\boldsymbol{q}$ and $\xi$ separately.

*4.4.2. Dynamic finite size scaling.* Two major practical limitations on the computer simulation of dynamic behaviour are finite evolution time and finite system size. The range of $\boldsymbol{q}$ for which data can be taken is limited, because of finite $L$, to values typically larger than those which is accessible to experiment. The method of analysis used in experiment is thus not effective here; instead the finite-size effect can be used directly to extract the dynamic critical exponent as has been done for statics (Landau 1990, Chen and Landau 1994). The divergence of the correlation length $\xi$ in the critical region is limited by the linear dimension of the system, $L$. Replacing $\xi$ by $L$ in the previous equations, and including the resolution function parameter $\delta_\omega$, we find

$$\int_{-\bar{\omega}_m}^{\bar{\omega}_m}\bar{S}^{\kappa}_L(\bar{q},\omega)\frac{\mathrm{d}\omega}{2\pi} = \tfrac{1}{2}\bar{S}^{\kappa}_L(\bar{q}) \tag{4.16}$$

with $\bar{S}^{\kappa}_L(\bar{q}) = \int_{-\infty}^{\infty} \bar{S}^{\kappa}_L(\bar{q},\omega)\mathrm{d}\omega/2\pi$ and

$$\bar{S}^{\kappa}_L(\bar{q},\omega) = \omega^{-1}\bar{S}^{\kappa}_L(\bar{q})\, F(\omega/\omega_m, qL, \delta_\omega/\omega_m) \tag{4.17}$$

where $F$ is a function which depends on $f$. We can then express $\bar{S}^{k}_L(\bar{q},\omega)$ in a scaling form,

$$\frac{\omega\bar{S}^{k}_L(\bar{q},\omega)}{\bar{S}^{k}_L(\bar{q})} = G(\omega L^z, qL, \delta_\omega L^z) \tag{4.18}$$

where $G$ is another unknown function. The median frequency $\bar{\omega}_m$ should then scale as

$$\bar{\omega}_m = L^{-z}\bar{\Omega}(qL, \delta_\omega L^z) \tag{4.19}$$

where the explicit form for function $\bar{\Omega}$ is also unknown. The different quantities, $\bar{S}^{k}_L(\bar{q},\omega)$, $\bar{S}^{k}_L(\bar{q})$ and $\bar{\omega}_m$, can be measured by simulations and used to test dynamic scaling and estimate the dynamic critical exponent $z$. The difficulty in choosing a shape function is avoided since the characteristic frequency can be estimated without that knowledge.

It is generally preferable to use (4.19), rather than (4.18), to determine the dynamic critical exponent $z$ due to the statistical fluctuations in $\bar{S}^{k}_L(\bar{q},\omega)$; these can be more or less averaged out in determining $\bar{\omega}_m$ by the integration and the normalization. Because the explicit form for function $\bar{\Omega}$ in (4.19) is generally unknown, $z$ may be extracted by self-consistent iterations. If the two arguments of the function $\bar{\Omega}$ are held fixed, then

$$\bar{\omega}_m \propto L^{-z}. \tag{4.20}$$

For the first argument of $\bar{\Omega}$, the product of $\boldsymbol{q}$ and $L$ is fixed, since we are interested in only those $q$ values determined by the periodic boundary conditions, i.e.

$$q = n_q(2\pi/L) \qquad n_q = 0, 1, 2, \ldots, L. \tag{4.21}$$

For the second argument, we choose

$$\delta_\omega = a(40/L)^z \tag{4.22}$$

where, with $t_{max} = 100/J$, $a = 0.025$, in units of $J$, was chosen empirically to provide a good compromise between effectively reducing the 'cutoff' oscillations and not excessively broadening the structure of the $S(q,\omega)$. An initial value $z^{(0)}$ is picked and used to determine $\delta_\omega$ by (4.22) for different $L$. Then $\bar{S}^{k}_L(\bar{q},\omega)$ and $\bar{\omega}_m$ are calculated for different combinations of $L$ and $q$ with $n_q$. A new estimate, $z^{(1)}$, can then be extracted from the simple relation (4.20), which is a special case of (4.19) with the function $\bar{\Omega}$ kept constant.

This process can be further simplified if the time integration can be carried out to long enough time that no resolution function is necessary. Then, (4.18) and (4.19) simplify to

$$\frac{\omega\bar{S}^{k}_L(\bar{q},\omega)}{\bar{S}^{k}_L(\bar{q})} = G(\omega L^z, qL) \tag{4.23}$$

and

$$\bar{\omega}_m = L^{-z}\bar{\Omega}(qL). \tag{4.24}$$

Thus, $z$ is given by the slope of a graph of log $\omega_m$ against log $L$ at fixed value of $qL$. Alternatively, (4.23) implies that for correctly chosen $z$ and for a fixed value of $qL$, graphs of $S^{kk}_L(q,\omega)/\{L^z S^{kk}_L(q)\}$ against $\omega L^z$ should all fall onto the same curve for different lattice sizes. Both procedures will only be valid for sufficiently large lattice size

## 5. Results and comparison with theory and experiment

### *5.1. One-dimensional XY model in a symmetry breaking field*

Arguably the most famous set of experimental measurements of a '1D' magnetic system are those shown in figure 2 for $CsNiF_3$ (Kjems and Steiner 1978). There were some disagreements between theoretical predictions and the experimental results, but whether was unclear whether this was a deficiency of the theory or a deficiency of the model used. From the results obtained from the spin dynamics simulations, shown in figure 3, it is clear that there is good overall qualitative agreement between the results for the ferromagnetic $XY$ chain in a transverse field and the theoretical mapping onto the sine–Gordon equation. There are quantitative differences in peak half-widths and intensities, however, and these limit to some extent the agreement that can be expected between the analytic theory and experiment. The experimental data had limited resolution and the different polarizations could not be measured directly. We note that $2\pi$ solitons could be observed directly in the simulations. Spin dynamics simulations for the corresponding antiferromagnetic $XY$ chain (Staudinger *et al* 1985, Gerling and Landau 1992) showed a more complicated dynamic structure factor than for the ferromagnet. Even more intriguing was the discovery of multiple kinds of '$\pi$-soliton' including one type that had not even been predicted theoretically.

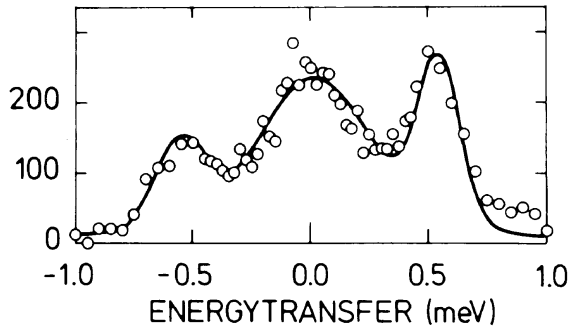


**Figure 2.** Inelastic neutron scattering data for $CsNiF_3$ in a transverse field. The open circles are the data with the background subtracted; the solid curve a is fit to the data using Lorentzian spin wave peaks and a Gaussian central peak. (From Kjems and Steiner 1978.)

### *5.2. Two-dimensional easy-plane magnets and the XY model*

Inelastic neutron scattering experiments have been carried out on several different layered materials which can generally be described as anisotropic 2D Heisenberg models, and these generally prove to be the closest physical realizations of the $XY$ model. These include $Rb_2CrCl_4$ (Hutchings *et al* 1986, Bramwell *et al* 1988) and $BaNi_2(PO_4)_2$ (Regnault *et al* 1983). The highest resolution experimental studies have been carried out on stage 2 $CoCl_2$ intercalated graphite (Wiesler *et al* 1994) and find four temperature regimes with different behaviour. There are indications of a Kosterlitz–Thouless transition at a temperature '$T_u$', though some properties disagree with KT predictions. For '$T_l$'$< T <$'$T_u$', they observe spin-wave peaks, but it is not clear whether a central peak is present. (In this region the long range part of the scattering function shows true 2D character, whereas for $T <$'$T_l$' 3D correlations develop.) Above '$T_u$', the in-plane scattering function shows the expected central peak, and the out-of-plane function exhibits damped spin waves. (In figure 10 we will show intensity

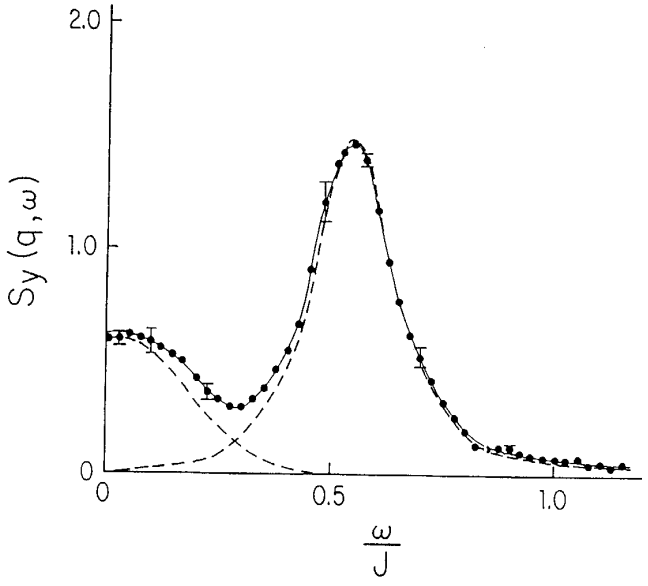


(*a*)

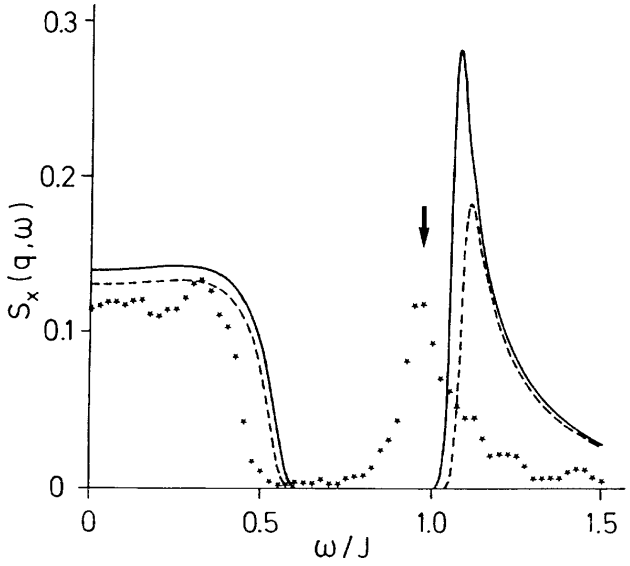


(*b*)

**Figure 3.** Spin dynamics data for $S(q,\omega)$ for a 1D $XY$ model: (*a*) $T = 0.4J/k$, $h = 0.1J$, $q = \pi/8$. The dashed lines are fits of a resolution broadened Gaussian central peak and a Lorentzian spin-wave peak. (*b*) $T = 0.2J/k$, $h = 0.1J$, $q = \pi/8$. The solid curve is the prediction from the sine–Gordon model; the dashed line uses the dispersion relation from the harmonic approximation. (From Gerling and Landau 1990.)

data from inelastic neutron scattering and make a direct comparison with both theory and simulation.) Although the resolution is not as good as for the simulations, one can see the

development of overdamped spin waves just above '$T_u$' and the presence of both a spin-wave peak and a central peak well below $T_u$. We should perhaps note here that there is experimental evidence that both defects as well as residual 3D coupling limit the 'effective size' of the 2D $XY$-like system to of the order of 100 lattice spacings. Further discussion and an extensive listing of relevant literature can be found elsewhere (Wiesler *et al* 1994).

Spin dynamics simulations for easy-plane Heisenberg magnets ($0 < \lambda < 1$, $D = 0$, and $H = 0$) in $d = 2$ have examined the contribution of vortices, spin waves and their interaction to the dynamic structure factor although much of this work is of modest quality. For $T > T_{KT}$ they have served as the major test of the phenomenological ideal vortex gas picture of the dynamics in $d = 2$ magnets (Mertens *et al* 1987, 1988, 1989). Kawabata *et al* (1986) and Landau and Gerling (1992) simulated the $XY$ model ($\lambda = 0$) with $L \leqslant 204$ and found both spin-wave peaks and a central peak. The resolution was too limited, however, to allow quantitative comparison with theory or to estimate the dynamic exponent. Simulations show that $S_{xx}(\boldsymbol{q}, \omega)$ and $S_{zz}(\boldsymbol{q}, \omega)$ behave differently. $S_{xx}(\boldsymbol{q}, \omega)$ is globally sensitive to the presence of vortices (Mertens *et al* 1987, 1988, 1989). In real space–time each vortex which passes a line connecting the origin $(\mathbf{0}, 0)$ and $(\boldsymbol{r}, t)$ becomes visible as a 'kink' in $S_{xx}(\boldsymbol{r}, t)$, i.e., $S_{xx}(\boldsymbol{r}, t)$ changes its sign when $(\boldsymbol{r}, t)$ passes through a vortex core. According to this picture the shape of $S_{xx}(\boldsymbol{q}, \omega)$ is given by a squared Lorentzian, (2.25), in which the Kosterlitz–Thouless correlation length $\xi$ shows up as the dominant length scale. This picture has been supported by spin dynamics simulations for $\lambda = 0$ ($XY$ model) (Mertens *et al* 1987, 1988); the line width and the integrated intensity of the central peak agree well with the phenomenological theory. For wave vectors $q \gg \xi^{-1}$ the spin-wave contribution to the intensity exceeds the vortex contribution, which decays as $q^{-3}$ in this regime (Mertens *et al* 1989). The vortex gas theory only works on length scales much larger than the vortex core radius $r_v$, so that $q \ll r_v^{-1}$ is required in (2.25) and therefore the $q$ range in which the vortex gas theory yields an adequate description shrinks. This has also been confirmed by spin dynamics simulations (Mertens *et al* 1989). In the limit $\lambda \to 1$ the vortex gas description finally becomes invalid for any $\boldsymbol{q}$. In contrast, $S_{zz}(\boldsymbol{q}, \omega)$ is locally sensitive to the presence of vortices. If one considers only incoherent scattering from independent vortices, the vortex gas theory yields a Gaussian central peak in $S_{zz}(\boldsymbol{q}, \omega)$ at high temperature, see (2.26). Spin dynamics simulations show that the linewidth is linear in $\boldsymbol{q}$; however, from vortex gas theory $S_{zz}(\boldsymbol{q}, \omega) = 0$ for $\lambda = 0$ ($XY$ model) in clear disagreement with the simulations which still give strong evidence for a distinct central peak in $S_{zz}(\boldsymbol{q}, \omega)$. More recent simulations show that the central peak only appears for $\lambda > \lambda_c$ (Costa and Costa 1996), although this conclusion has been questioned (Gouvêa and Wysin 1997). Strong fluctuations in the number of vortices as a function of time suggest that vortex–anti-vortex pair creation/annihilation may be responsible for the central peak. The phenomenological vortex gas picture can thus only be used as a first approximation to out-of-plane correlations when $\lambda$ is large enough.

To further determine the role which vortices play in $d = 2$ magnets, detailed simulations of the vortex dynamics have been performed (Wysin 1990, Wysin *et al* 1988, Gouvêa *et al* 1989) with spin waves suppressed by the introduction of Landau–Gilbert damping in the equations of motion. As initial configurations single vortices or vortex–anti-vortex pairs were chosen on different lattices and the simulations performed at constant energy and at fixed temperature, but averages were taken over only three initial configurations. Planar vortices are stable for anisotropies $\lambda < \lambda_c$ and develop out-of-plane components only for $\lambda > \lambda_c$. Likewise, an out-of-plane vortex relaxes to an in-plane vortex for $\lambda \leqslant \lambda_c$ and is stable only for $\lambda > \lambda_c$. More detailed simulations find that $\lambda_c \simeq 0.71$ for a square lattice (Costa and Costa 1996). A planar vortex pair is stable if the initial separation between the vortices is large enough (typically half the linear lattice size) and $\lambda \leqslant 0.7$ (square lattice). For small initial separations out-of-

plane components develop from an initial in-plane configuration. For $\lambda \geqslant 0.8$ out-of-plane components even develop for a large initial separation; the vortex and the anti-vortex move towards one another along spiral trajectories and may finally annihilate each other. These simulations indicate that correlations in the out-of-plane spin motions emerge from moving planar vortices rather than exclusively from static vortices with out-of-plane components. According to this modified vortex picture $S_{zz}(\boldsymbol{q}, \omega)$ still shows the Gaussian central peak in (2.26). The line width is linear in $q$ as in (2.26) which is supported by the simulation data ($T > T_{KT}$) (Gouvêa *et al* 1989). The integrated intensity agrees with the Monte Carlo data to within the order of magnitude. Whether the line shape is really Gaussian, however, cannot be decided on the basis of the numerical data. More complete simulations have now been performed with much higher statistics for $\lambda = 0$ ($XY$ model) (Evertz and Landau 1996) which will be described later in this section.

The motion of vortex pairs has also been studied for easy-plane antiferromagnets (Völkel *et al* 1991a), where the vortices in non-stationary vortex pairs move towards one another on straight rather than spiral trajectories. The reason is that the spins in the out-of-plane component of a vortex are antialigned in an antiferromagnet and do therefore not produce an effective magnetic field between the vortices. As in the case of easy-plane ferromagnets the vortices are almost in plane for $\lambda \leqslant \lambda_c$, where $\lambda_c \simeq 0.71$ for a square lattice. The dynamic correlations in easy-plane antiferromagnets are somewhat more complicated than in their ferromagnetic counterpart. This is on one hand due to the presence of two distinct spin-wave branches, namely an in-plane (optical) branch and an out-of-plane (acoustic) branch. On the other hand spins in vortices are antialigned rather than aligned so that for $\lambda < \lambda_c$ the static vortex structure ($T > T_{KT}$) leads to a central peak at $\boldsymbol{q} = (\pi, \pi)$ in $S_{xx}(\boldsymbol{q}, \omega)$, just where the dispersion of the optical branch has its zero. Spin-wave contributions to $S_{xx}(\boldsymbol{q}, \omega)$, however, vanish completely at this $\boldsymbol{q}$ value. Motion of free vortices for $T > T_{TK}$ produces a central peak at $\boldsymbol{q} = (0, 0)$ in $S_{zz}(\boldsymbol{q}, \omega)$ apart from a distinct spin wave peak which remains visible even above $T_{KT}$. For $\lambda > \lambda_c$ out-of-plane vortices with antiferromagnetic structure are stable (Völkel *et al* 1991a) so that vortex peaks are expected to appear at $\boldsymbol{q} = (0, 0)$ and $\boldsymbol{q} = (\pi, \pi)$ in both $S_{xx}$ and $S_{zz}$. For $\lambda = 0$ and $T > T_{TK}$ the simulation data for the central peak in $S_{xx}$ are well described by a squared Lorentzian shape function (see (2.25) for $\boldsymbol{q} \to (\pi, \pi) - \boldsymbol{q}$). The $q$ dependence of the line width and the integrated intensity are in good agreement with vortex theory in the temperature range $T_{KT} \leqslant T \leqslant 1.25 T_{KT}$. Above $1.25\ T_{KT}$ diffusive spin motion begins to dominate. As in the previous cases the predicted Gaussian line shape of the central peak in $S_{zz}$, see (2.26), cannot be uniquely verified, because the spin-wave peak dominates for most of the $q$ values. However, for small $q$ the simulation yields a line width which is consistent with the analytic prediction (Völkel *et al* 1991b). Spin dynamics simulations of a 2D $XY$ model in a transverse magnetic field (Gouvêa *et al* 1990) suggest that $S_{xx}$ is more sensitive to domain walls whereas $S_{yy}$ and $S_{zz}$ are to vortices. Spin dynamics simulations have also been used to investigate the isotropic antiferromagnet ($\lambda = 1$) in $d = 2$ near the antiferromagnetic Bragg point $\boldsymbol{q} = (\pi, \pi)$ (Wysin 1990). From the isotropy of the model it is evident that all components of the dynamic structure factor are equivalent. This symmetry also implies that $S(\boldsymbol{q}, \omega)$ is well described by a product of symmetrically located Lorentzians for $\boldsymbol{q}$ values close to $(\pi, \pi)$. The simulation data agree with this peculiar line shape.

The most complete simulations of an easy-plane ferromagnet are for $\lambda = 0$ ($XY$ model) by Evertz and Landau (1996) who studied $L \times L$ lattices with periodic boundary conditions for $16 \leqslant L \leqslant 192$, both below and above $T_{KT}$. Equilibrium configurations were created at each temperature using a hybrid Monte Carlo method which combined cluster updates of the $x$ and $y$ spin components (using the Wolff embedding method) (Swendsen *et al* 1992) with vectorized Metropolis and overrelaxation spin reorientations (Landau 1992) to produce rapid

decorrelation of successive configurations. Between 500 and 1200 equilibrium configurations were generated for each lattice size and temperature, and the error bars in the figures represent statistical errors for averages over these configurations. The time integration was done using a vectorized fourth-order predictor–corrector method with $\Delta = 0.01/J$ and a maximum integration time of $t_{max} = 400/J$. To reduce memory and CPU time, only momenta $\boldsymbol{q} = (q, 0)$ and $(0, q)$ were calculated, with $q$ determined by the periodic boundary conditions (see (4.21)), and data from these two spatially equivalent directions were averaged together to enhance the statistical accuracy. Fast Fourier transforms were used to calculate correlation functions. For $T \leqslant T_{KT}$ the $XY$ model is critical and the dynamic exponent $z$ can be extracted using dynamic finite size scaling theory. For this analysis no resolution function was needed to smoothen the effects of finite $t_{max}$ because of the long integration times.

The results of the initial analysis prompted additional static Monte Carlo studies which provided an improved estimate of $T_{KT} = 0.700(5)$; additional (but less extensive) spin dynamics simulations were then performed there. Figure 4 shows the temperature dependence of $S(q, \omega)$ as a function of $\omega$, for $L = 192$ and fixed, small momentum $q = \pi/48$, i.e. $n_q = 2$ in (4.21). $S_{xx}(q, \omega)$ exhibits a very strong and moderately sharp spin-wave peak at temperatures $T \leqslant T_{KT}$. The position of the peak moves towards lower frequency as the temperature increases, and the peak broadens slightly. Just above the transition, at $T = 0.725$ there is still both a strong spin-wave peak and a sizable central peak, but at higher temperature, the spin-wave peak disappears (for this small $q$) and only a large central peak remains. Note that from KT theory one would expect complete disappearance of a spin-wave peak at all $T \geqslant T_{KT}$. There is additional structure in $S^{xx}$ away from the spin-wave peak at temperatures up to $T_{KT}$.

$S^{zz}(q, \omega)$ has structure with two orders of magnitude less intensity than the in-plane component. There is a very sharp spin-wave peak for $T \leqslant T_{KT}$, whose width is limited by the $\omega$ resolution, with noticeable finite time cutoff induced oscillations. The oscillations can be smoothened by convoluting $S(q, \omega)$ with a Gaussian resolution function, as shown in the inset; but this also masks the sharp nature of the spin-wave peak. No central peaks are visible in $S^{zz}(q, \omega)$ for $T \leqslant T_{KT}$, and, in contrast to $S^{xx}(q, \omega)$, there is a clear, but weak, spin-wave peak at all temperatures, even above $T_{KT}$. Below the transition, the intensity of the spin-wave peak depends strongly on lattice size, whereas its position is constant. For $T = 0.725$, the spin-wave peak in $S^{xx}(q, \omega)$ appears to gain intensity slightly as $L$ increases, whereas neither the central peak nor the spin-wave peak in $S^{zz}(q, \omega)$ show any finite size effects. At higher temperature there is no visible lattice size dependence in either $S^{xx}(q, \omega)$ or $S^{zz}(q, \omega)$.

The position of the spin-wave peak is the same for $S^{xx}(q, \omega)$ and $S^{zz}(q, \omega)$ and is proportional to momentum for small $q$. As $q$ increases, the peak broadens, and becomes less intense, yet it remains quite well defined. For the $zz$ component, both the total intensity and the relative loss of intensity with increasing momentum are much smaller. We conclude that $S^{zz}(q, \omega)$ has the expected delta function form only for very small $q$.

Well above $T_c$, at $T = 0.8$, $S^{xx}(q, \omega)$ has no noticeable spin-wave peak at small $q$, and the strong central peak rapidly loses intensity with increasing $q$. In marked contrast, the behaviour of $S^{zz}(q, \omega)$ maintains a clear but broadened spin-wave peak although there is also non-zero intensity at small $\omega$ in $S^{zz}(q, \omega)$. Surprisingly, even at this temperature spin waves appear in $S^{xx}(q, \omega)$ for very large momenta so that both a central peak and a spin-wave peak are present. Note that the scale in figure 4(b) is about 100 times smaller than in figure 4(a). Figure 5 shows the position $\omega_p$ of the spin-wave peak as a function of momentum. The expected linear portion of the dispersion curve extends to rather large momenta. With increasing temperature, the spin-wave phase velocity $\omega_p/q$, which is proportional to the spin-wave stiffness, decreases slowly and approximately linearly, as shown in the inset, and theoretically expected for small

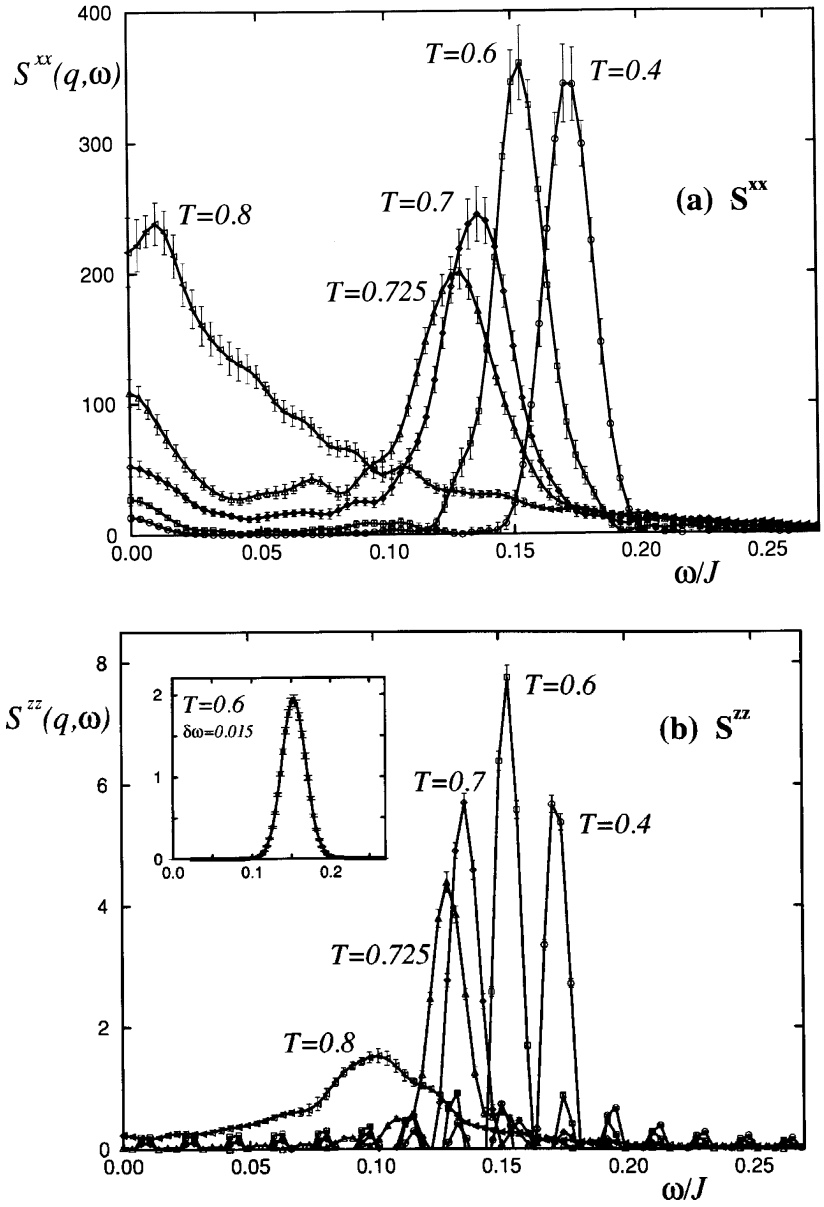


**Figure 4.** Spin dynamics data for the 2D $XY$ model. Note $T_{KT} = 0.700(5)$. $L = 128$ and $n_q = 2$ in all cases: (a) transverse component; (b) longitudinal component; the inset shows data at $T = 0.6$, smoothed with a resolution function. (From Evertz and Landau 1996.)

$T$ (Nelson and Kosterlitz 1977). Above $T_{KT}$ we can only plot the position of the residual peak in $S^{zz}(q, \omega)$; the $xx$ component has dropped sharply to zero.

Below $T_{KT}$ the data for $S^{xx}(q, \omega)$ show additional very small peaks with intensities typically $10^{-2}$ of that of the spin-wave peaks. No such structure can be found in $S^{zz}(q, \omega)$. At each temperature the locations of the small peaks are essentially unchanged with $L$ for fixed $n_q = qL/(2\pi)$. One simple explanation which is consistent with the data, but for

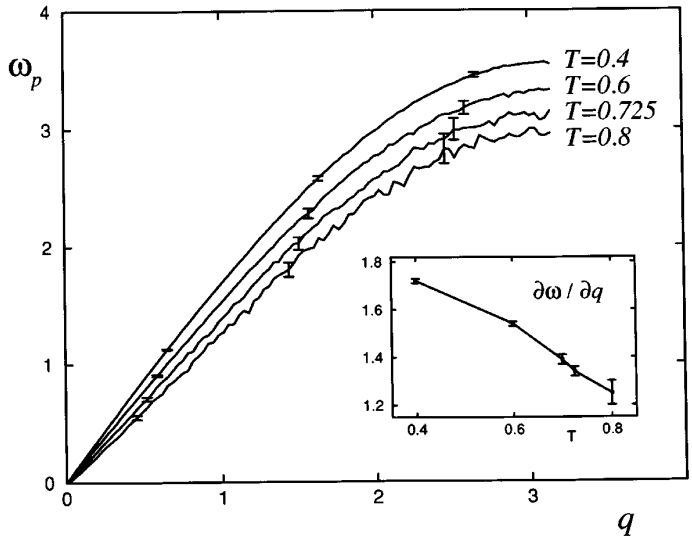


**Figure 5.** Spin dynamics results for the frequency $\omega^{xx}$ for the 2D $XY$ model: spin wave against momentum, for $L = 192$. Note that at $T = 0.8$ only $S^{zz}(q, \omega)$ has a spin-wave peak. The inset shows the temperature dependence of the spin-wave velocity $\partial\omega/\partial q$. (From Evertz and Landau 1996).

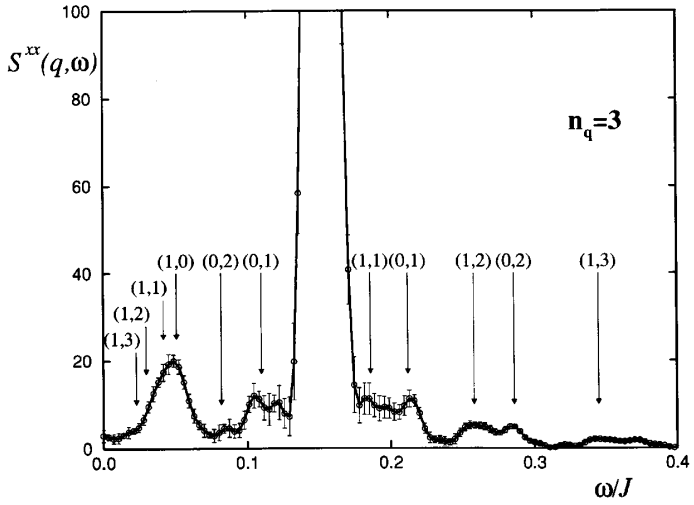


**Figure 6.** Spin dynamics data for the 'fine structure' in $S^{xx}(q, \omega)$ for the 2D $XY$ model for $T = 0.6$, $L = 192$, $n_q = 3$; vertical arrows show the expected location of two-spin-wave peaks. The single-spin-wave peak volume is about 300. (From Evertz and Landau 1996.)

which we have no rigorous theory, is two-spin-wave effects. $S(q, \omega)$ should show a single spin-wave peak at a characteristic frequency $\omega_p$ plus additional sum and difference peaks due to two-spin-wave processes involving total momentum $q$. The resultant positions of the excitations involving the most likely (i.e. smallest individual $q$ value) excitations for the case of $n_q = 3$ and $T = 0.6$ are marked in figure 6 and identified by the coordinates of the

first vector in reciprocal space; the sum of the two spin-wave momenta must equal $q = 3\ (2\pi/L)$. The locations of the resultant excitations agree extremely well with the positions of the small peaks in $S(q, \omega)$, but there is no way of comparing intensities. Interpolating the intensities for odd values of $n_q$ (which do not show peaks at $\omega = 0$) to obtain estimates for even $n_q$, we conclude that there is extra intensity at $\omega = 0$ which is *not* attributable to two spin waves.

The characteristic frequency $\omega_m$ of the whole spectrum of $S(\boldsymbol{q}, \omega)$ is defined by (4.16). When there is only a single spin-wave peak, then $\omega_m$ coincides with the spin-wave frequency $\omega_p$, e.g. for $T = 0.4$. Closer to the transition, intensity between $\omega = 0$ and $\omega_p$ grows; therefore the characteristic frequency $\omega_m^{xx} < \omega_p$. The dynamic exponent $z$ can be extracted by analysing $\omega_m$, or by looking at $S(\boldsymbol{q}, \omega)$ itself. In figure 7 we show $\omega_m^{xx} L^z$ as a function of $qL$, for $T \leqslant T_{KT}$ using $z = 1.0$. The data show good scaling behaviour for both temperatures. The asymptotic behaviour for large $L$ is strictly linear, $\omega_m L^z \sim qL$, i.e. for $z = 1$, $\omega_m \sim q$. For each finite lattice size the dispersion curve flattens when $q$ becomes large. Therefore as $L$ increases, the

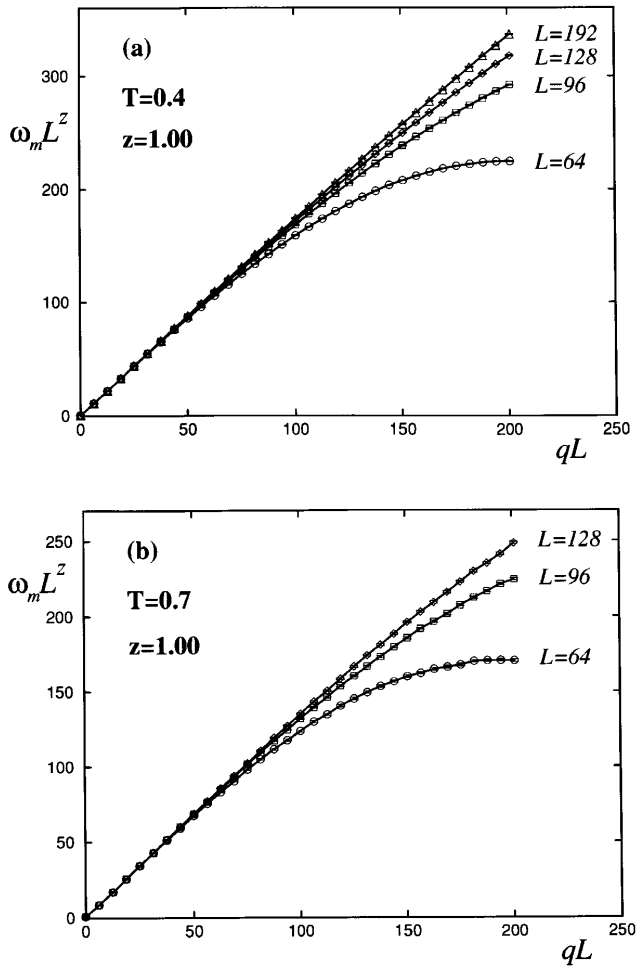


**Figure 7.** Finite size scaling of the characteristic frequency for the 2D $XY$ model determined from spin dynamics simulations; $\omega_m^{xx} L_z$ is plotted against $qL$. (From Evertz and Landau 1996.)

data start to move away from the asymptotic behaviour at progressively larger values of $qL$. For different values of $z$ the data do not fall onto a common line even at the smallest momenta. Remarkably, the scaling curves for $\omega_m^{xx}$ at all $T \leqslant T_{KT}$ are similar, with variation only in their slope. In contrast to this, we do not observe similar scaling behaviour in $\omega_m^{xx}$ at $T > T_c$.

For $q \neq 0$, $\omega_m^{zz}$ has the same scaling behaviour as the in-plane component. At $T = 0.4$ the data are indistinguishable, but as intensity below the spin-wave peak grows at higher $T$, the scaling curve for $\omega_m^{zz}$ develops a larger slope than $\omega_m^{xx}$. Interestingly, at $T = 0.8$, above the transition, not only are there spin-wave peaks in present in $S^{zz}(q, \omega)$, but $\omega_m^{zz}$ also shows 'effective' scaling behaviour as below the transition, with $z = 1.0$.

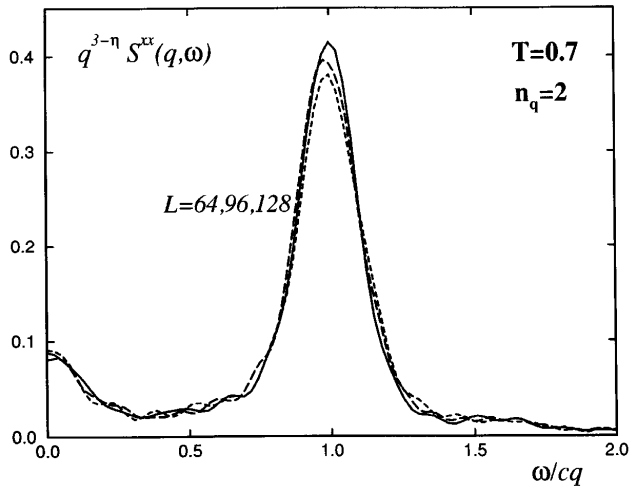


**Figure 8.** Finite size scaling of spin dynamics results for the transverse dynamic structure factor $S^{xx}$ for the 2D $XY$ model; $\omega S(q, \omega)/S(q)$ is shown versus $\omega L^z$, with constant $n_q$. The curves correspond to different lattice sizes. (From Evertz and Landau 1996.)

If dynamic finite size scaling holds, then the scaled dynamic structure factor should fall onto a single curve for sufficiently large lattices. Figure 8 shows a scaling plot for $S^{xx}(q, \omega)$; for all $T \leqslant T_{KT}$ the data do indeed fall onto a single curve, when $z = 1.00$. Only data from very small $L$ (not shown here) deviate systematically. Note that scaling with $\omega L^z$ implies that at fixed $qL$ the spin-wave peak for large $L$ is very narrow. Its width is therefore very sensitive to $t_{max}$ in the spin dynamics integration, thus necessitating very long time integrations. The scaling behaviour is very sensitive to variations in $z$ leading to errors bars which are less than 3%. Note that $z$ is the same across a range of temperature for which the static exponent $\eta$ varies strongly, from $\eta = 0.082(1)$ at $T = 0.4$ to $\eta = 0.247(6)$ at $T = 0.700$. $S^{zz}(q, \omega)$ is extremely narrow at $T = 0.4$ and $T = 0.6$, and cannot show scaling given the $t_{max}$ used, but at $T = 0.700$ the spin-wave peak in $(q, \omega)$ has broadened and scaling is verified. Figure 9 compares the results with theoretical predictions for the shape of $S(q, \omega)$. Neither the prediction by Nelson and Fisher (1977) nor by Moussa and Villain (1976) describe the data well. Both predicted lineshapes exhibit a much narrower and higher spin-wave peak than the data, even when we take into account the widening of the data due to the finite time cutoff, and neither show a central peak. The prediction by Moussa and Villain also decays too slowly at high frequencies. Inelastic neutron scattering data for $CoCl_2$-GIC show the development of both a spin-wave peak and a broad central peak. Neutron scattering data (Hutchings *et al* 1986) for $Rb_2CrCl_4$ have too much scatter to allow any quantitative comparison, although they have been interpreted

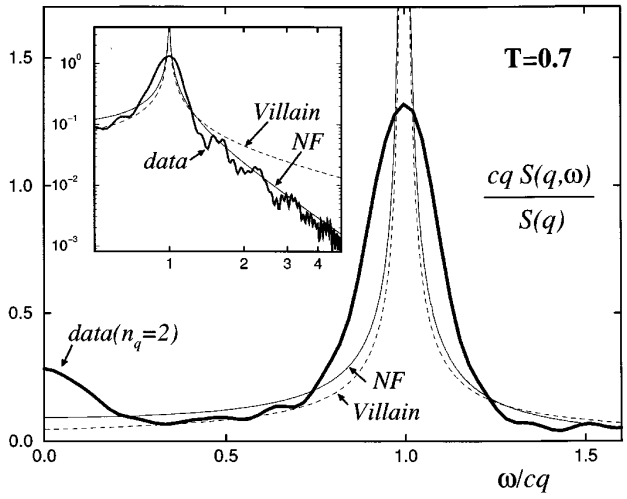


(*a*)

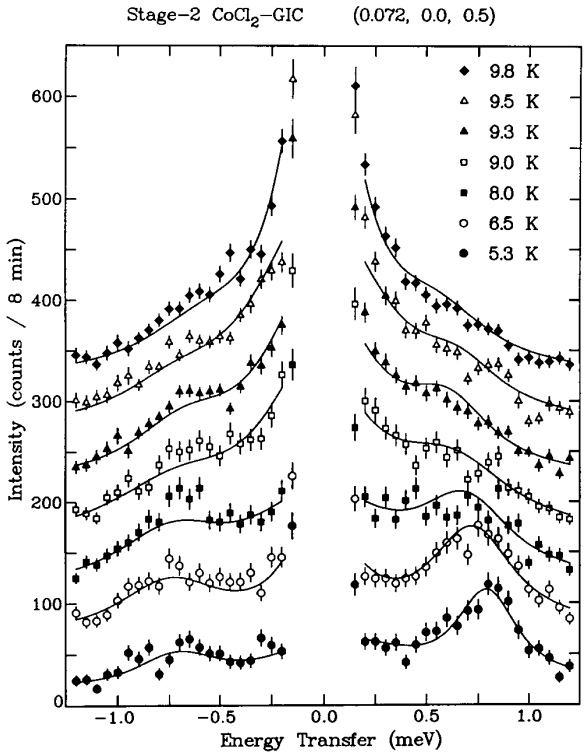


(*b*)

**Figure 9.** (*a*) Comparison of the spin dynamics lineshape for the 2D $XY$ model, $S^{xx}(q,\omega)$, with theoretical predictions, at $T = T_{KT}$, $L = 128$ and $q = \pi/32$. Thin curves represent predictions by Nelson and Fisher and by Villain (with $\eta = 0.25$ and with a suitably adjusted prefactor). (From Evertz and Landau 1996.) (*b*) Inelastic neutron scattering results for $CoCl_2$-GIC (from Wiesler *et al* 1994).

in terms of both spin-wave and central peaks. Magnetic scattering data (Regnault *et al* 1983) for $BaNi_2(PO_4)_2$ show a very pronounced central peak and a spin-wave peak, both primarily transverse in character.

The central peak has been ascribed to diffusion of vortices. This interpretation was called into question by Costa *et al* (1997) who studied both vortex motion as well as vortex creation/annihilation as a function of time. They find little vortex motion except at high temperatures; instead the vortices are rather quickly annihilated and recreated elsewhere.

### *5.3. Three-dimensional critical dynamics of the Heisenberg model*

*5.3.1. Isotropic systems.* Spin motions in the classical, $d = 3$ Heisenberg ferromagnet were studied almost three decades ago (Watson *et al* 1969), but the limited resolution possible at that time made quantitative analysis impossible ($t_{max}$ was limited to less than $20/J$). More recent simulations have shown that it is now possible to probe the critical regime. We remind the reader that dynamic scaling suggests that $z = d - \beta/\nu$ for class J, and various theories (Hohenberg and Halperin 1977, Wagner 1970, Freedman and Mazenko 1976, Cuccoli *et al* 1994) predict that $z = d/2$ for class G. Both systems have now been studied with spin dynamics methods using $L \times L \times L$ body-centred-cubic systems with periodic boundary conditions. The critical point is known accurately (Chen *et al* 1993), $T_c = 2.054\,241 J/k$.

Spin dynamics simulations for the ferromagnet were carried out for $16 \leqslant L \leqslant 40$. A fully vectorized, checkerboard hybrid algorithm (Landau 1992) was used to reduce critical slowing down and a vectorized fourth-order predictor–corrector method was used to perform the integration. A Cartesian coordinate system in spin space was chosen such that its $z$ axis was in the same direction as the magnetization of the spin configuration, and $t_{max} = 120/J$ with a time step $0.01/J$. For $T = T_c$ with $L = 40$, a variation only in the fifth digit of the total energy and in the sixth digit of the length of individual spins was observed.

At $T_c$ the magnetization survives because of finite size effects, and the transverse component and its longitudinal counterpart still behave slightly differently. Due to statistical fluctuations, finite size effects in $S(q, \omega)$ are not easily observable; however, systematic shifts in the peak position and in the magnitude of the wings of the transverse component can be seen. For the longitudinal part we can also observe a systematic change in the intensity at $\omega = 0$. It turns out, as we will see later, that a better way to look into the finite size behaviour is to draw a scaling plot according to (4.19) by fixing the values of $qL$ and $\delta_\omega L^z$. Because the behaviour of the transverse neutron scattering function $S_L^{\perp}(q, \omega)$ in the critical region is not complicated by the residual magnetization as is $S_L^{\parallel}(q, \omega)$, it is best suited for closer study. The temperature dependence of the spin-wave frequency, read directly from the peak position, in the vicinity of the critical point can be easily measured for different lattice sizes. Systematic rounding appears when $(1 - T/T_c) < 0.03$. This is clearly due to finite size effects, because this temperature range is so close to $T_c$ that the correlation length becomes limited by the linear dimension of the system. On the other hand, finite size effects seem to be negligible for the system with $L = 40$ further away from $T_c$. If finite size effects are negligible and the $q$ value is small and fixed, both mode-coupling theory and hydrodynamic theory (Wagner 1970, Cuccoli *et al* 1989) predict that the spin-wave frequency should vary as $(1 - T/T_c)^{\nu-\beta}$. Fits to data with $L = 40$ and $(1 - T/T_c) \geqslant 0.03$ for $n_q = 2, 3$ yield two estimates whose mean value gives $(\nu - \beta) = 0.316(21)$. Direct measurements give $(\nu - \beta) = 0.3409(65)$ so, within their respective error bars, results from static and dynamic properties are in good agreement. The dynamic critical exponent $z$ can be extracted from $\bar{\omega}_m$ by the iteration scheme described in the previous section. When applied at $T_c$ for $n_q = 2$, using two different initial values of $z^{(0)}$, the two iterations converge to $z = 2.498$. A similar analysis for $n_q = 3$ was made, and in

figure 10 the size dependence of $\bar{\omega}_m$ is plotted on a logarithmic scale. When not shown, the estimated error bars for individual points are smaller than the size of the points. Within their respective error bars, the two estimates for $z$ agree and yield an average of $z = 2.478(28)$. Experimentally, $z$ was estimated to be $2.50 \pm 0.07$ from inelastic neutron scattering data for EuO (Böni and Shirane 1986, Böni *et al* 1987); this value is consistent with the spin dynamics estimate but with a larger uncertainty.

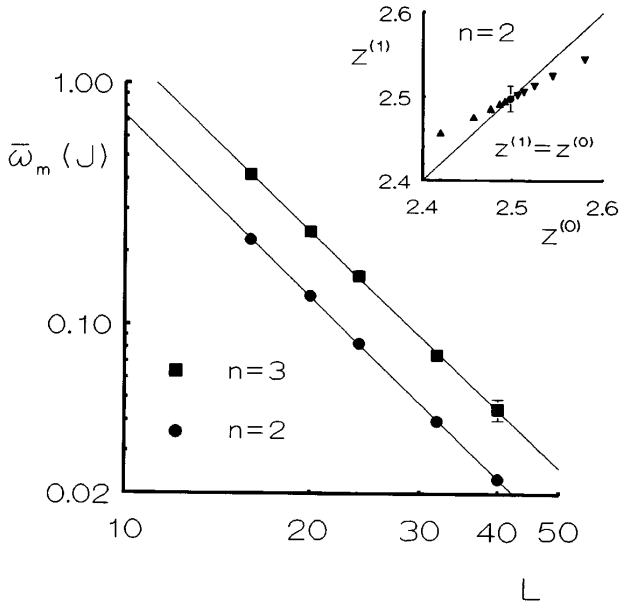


(*a*)

**Figure 10.** Determination of the dynamic critical exponent. (*a*) Finite size dependence of the median frequency obtained from spin dynamics data for $S(q, \omega)$ for the body-centred-cubic classical Heisenberg ferromagnet. The inset shows the result of the iterative analysis. (*b*) Neutron scattering data for the half-width for EuS (Böni *et al* 1987).

The dynamic finite size scaling behaviour of $S_L^{\perp}(q, \omega)$ is plotted in figure 11 for $n_q = 2$ with $z = 2.478$. The estimated error bars for individual data points are shown unless they are smaller than the size of the symbols. Within their respective error bars, data points collapse onto the same curve, thus supporting the estimate for $z$. With values of $\nu$ and $\beta$ which were obtained from a high-resolution Monte Carlo study of static critical behaviour the dynamic scaling law (Hohenberg and Halperin 1977) $z = 2 + (\nu - \beta)/\nu$ predicts $z = 2.4837(72)$. The dynamic result $(\nu - \beta) = 0.316(21)$, together with static result for $\nu$, yields $z = 2.448(32)$. Within their respective error bars, these two estimates are consistent and agree well with the value $z = 2.478(28)$ from dynamic scaling. The range of validity of dynamic scaling was found to be limited, i.e. for $q \geqslant 0.5/\pi$, e.g. $n = 4$ for $L = 16$, the data are outside the scaling (figure 11) regime. For comparison we note that a (Metropolis) Monte Carlo study of this model (Peczak and Landau 1993) yielded $z \sim 1.96$ for relaxational critical behaviour.

Spin dynamics simulations at high temperatures for an fcc Heisenberg ferromagnet (Chaudhury and Shastry 1988) found good agreement with neutron scattering data on EuO (Böni and Shirane 1986) and with the predictions of Young and Shastry (1982). They did not

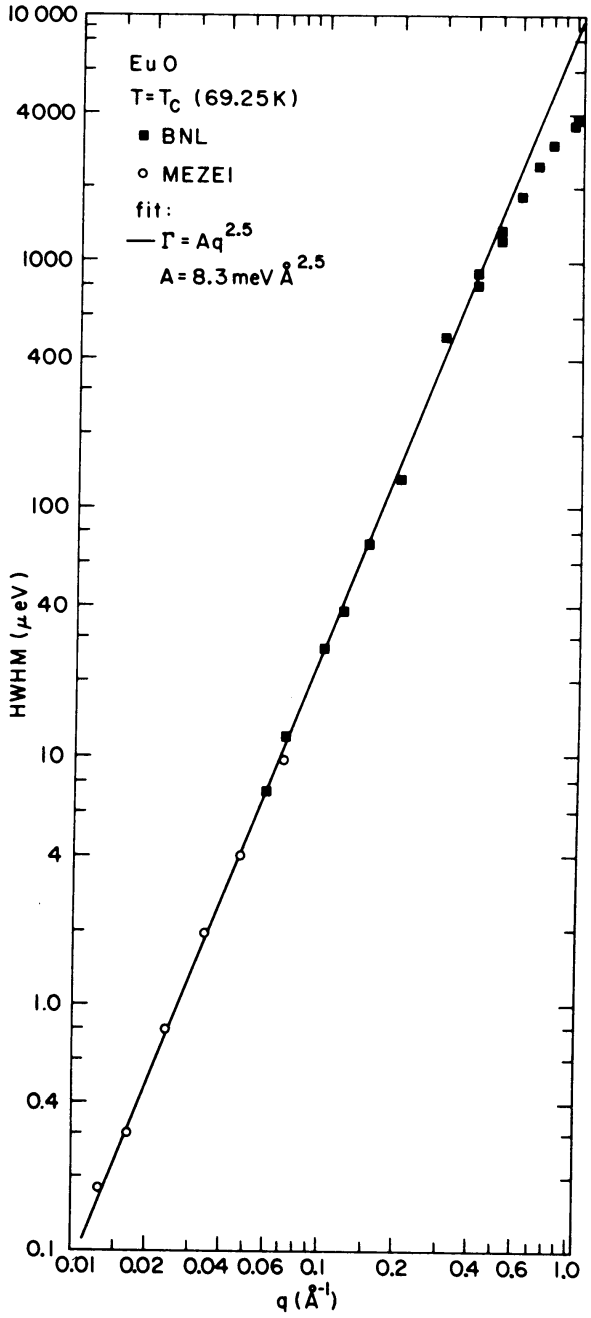


(*b*)

**Figure 10.** (Continued)

find the two-peak structure predicted by Lindgård (1983) near the zone boundary. Closer to $T_c$ dipolar effects become a consideration (Lovesey and Williams 1986, Balucani *et al* 1987),

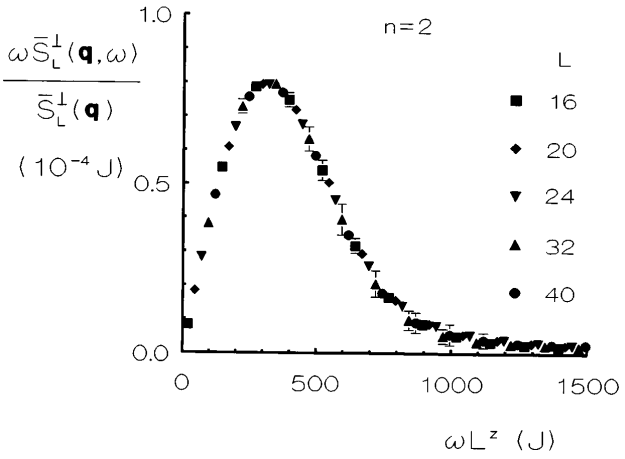


(*a*)

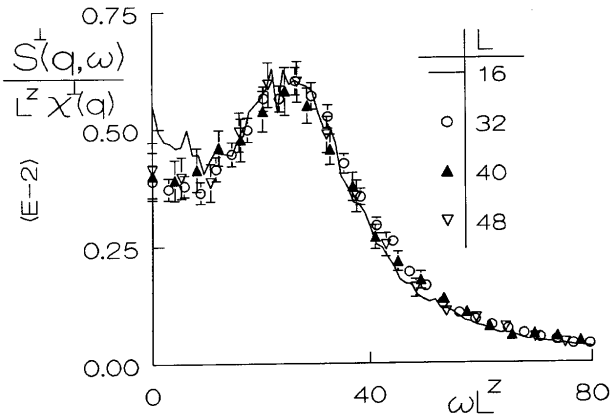


(*b*)

**Figure 11.** Dynamic finite size scaling of the transverse component of $S(q, \omega)$ for bcc Heisenberg magnets. (*a*) the ferromagnet with $n_q = 2$ and $z = 2.478$ (Chen and Landau 1994); (*b*) the antiferromagnet with $n_q = 2$ and $z = 1.48$ (Bunker *et al* 1996).

but no spin dynamics simulations have yet been performed with dipolar couplings.

Many of the qualitative features of the data obtained by spin dynamics for the antiferromagnet (Bunker *et al* 1996) were similar to those for the ferromagnet. Data are compared with experiment in figure 12. Below $T_c$ the spin-wave peak becomes narrower and increases in frequency, as expected, and it approaches linear spin-wave theory at low $T$. Peak widths even for $T = 1.0J$ are wide enough that the contribution due to the finite resolution is negligible. The longitudinal and transverse spin waves are at the same frequency; however the spin wave peak is much less intense in the longitudinal component than in the transverse component. This is to be expected since according to linear spin-wave theory longitudinal excitations vanish as $T \to 0$.

At $T_c$ the longitudinal component is similar in form to that of the Heisenberg ferromagnet with both a central peak and a spin-wave peak. As is the case for $T < T_c$ there is a much stronger central diffusion peak in the longitudinal component than in the transverse component. The

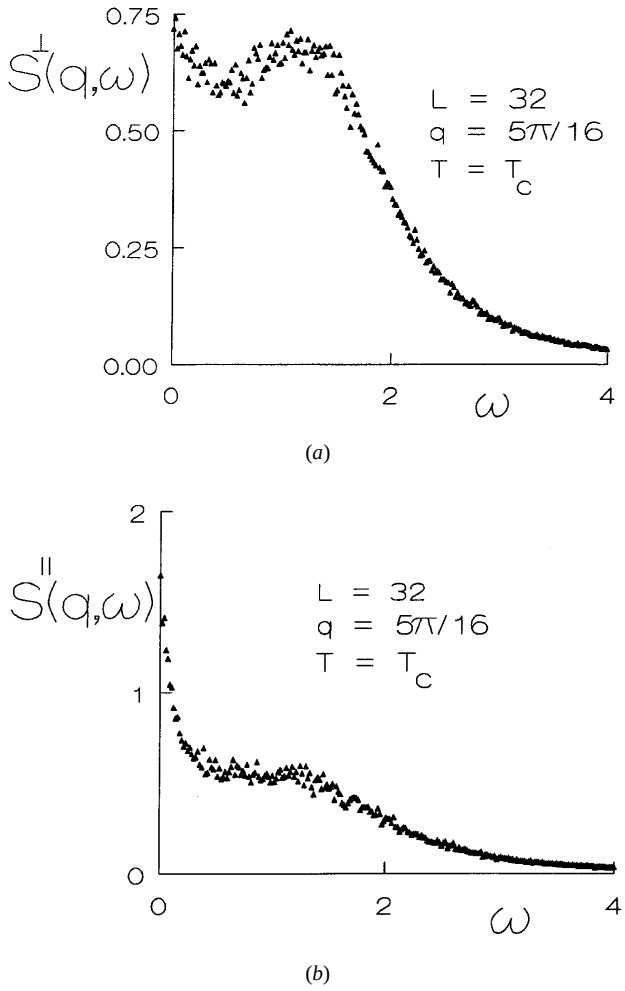


**Figure 12.** Spin dynamics data for $S(q, \omega)$ for the bcc Heisenberg antiferromagnet: (*a*) transverse component; (*b*) longitudinal component (Bunker *et al* 1996). (*c*) Inelastic neutron scattering data for $RbMnF_3$ (Tucciarone *et al* 1971).

spin-wave peak of the longitudinal component is also weaker than in the transverse component. When $q$ increases the overall intensity goes down and the spin-wave peak frequency increases and the peak broadens. While over most $q$ values the relative intensities of the central and spin-wave peaks remain constant, at very small $q$ the relative intensity of the central peak decreases. Finite size effects extend to larger $L$ for the central peak than for the spin-wave component, but no finite size effect is noticeable for $L$. Results for $S_L^{\perp}(q, \omega)$ are in qualitative agreement with the experimental results (Tucciarone *et al* 1971, Cox *et al* 1989, Coldea *et al* 1998) in that there is both a central peak as well as a spin-wave peak, but there appear to be pronounced quantitative differences between the two sets of neutron scattering data. The newer results (Cox *et al* 1989, Coldea *et al* 1998), taken just below $T_N$, show a much weaker central peak of clearly longitudinal nature. In contrast, as shown in figure 13, mode coupling theory (Cuccoli *et al* 1994) does not predict a central peak at $T_c$.

As expected the dispersion curve looks quite different for the antiferromagnet and the

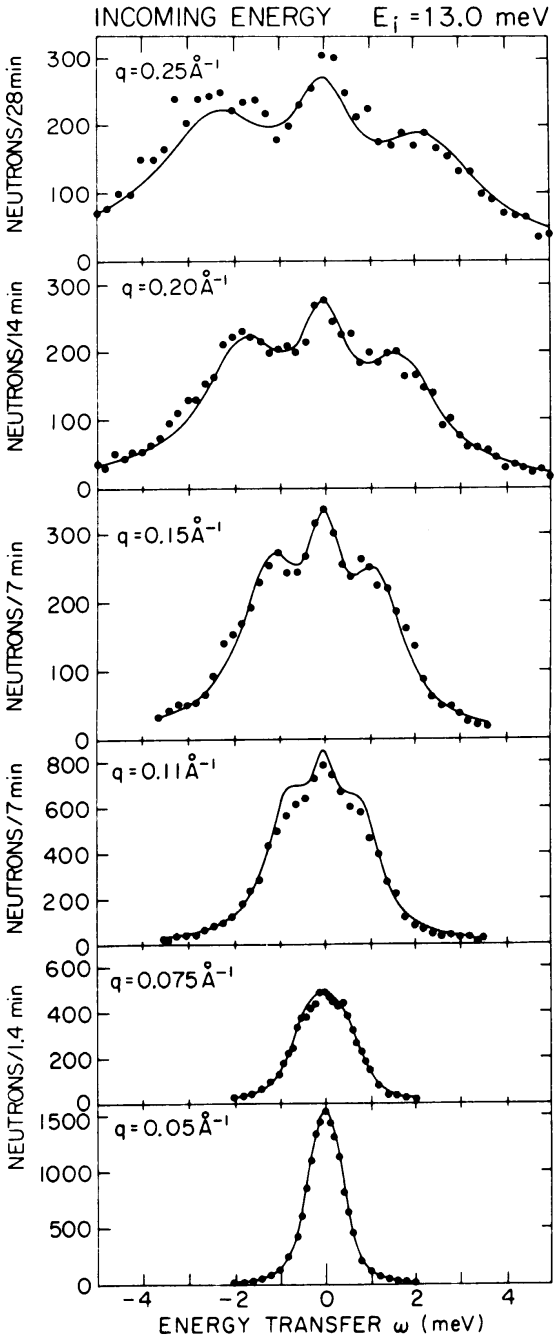


(*c*)

**Figure 12.** (Continued)

ferromagnet. (For small $q$ the spin-wave peak was completely hidden by the central peak.) The dispersion curve values we were able to obtain, however, show the decreased frequency

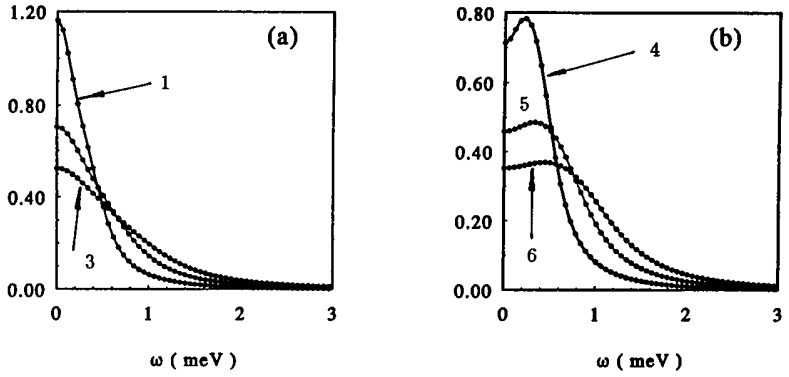


**Figure 13.** Dynamic structure factor at $T = T_c$ as predicted from mode–mode coupling theory for the isotropic Heisenberg antiferromagnet (AF). (a) Near the Brillouin centre; (b) near the AF-ordering wave vector $w = (1, 1, 1)$. The wave vectors in units of $(\pi/12a_0)$ are: 1, (0,0,1); 2, (0,1,1); 3, (1,1,1); 4, (11,12,12); 5, (11,11,12) and 6, (11,11,11). (Cuccoli *et al* 1994.)

as predicted by renormalization group theory (Freedman and Mazenko 1976).

In order to test the dynamic scaling theory $\omega_m(qL)$ was determined from $S_L^{\perp}(q, \omega)$ with fixed values of $qL$ for all lattice sizes. The integration times used for the antiferromagnet were long enough that the use of a resolution function was unnecessary and $z$ could be extracted directly without using the iterative procedure described earlier for the ferromagnet. If data for all $L$ are used to determine $z$ from the slope of the log–log plots of $\omega_m$ against $L$, a value of approximately $z = 1.4$ is obtained; however using only the three largest lattices one finds $z = 1.48(4)$. Clearly corrections to the asymptotic finite size effects are subtle and important. The estimate of $z = 1.48(4)$ agrees well with the experimental results (Tucciarone *et al* 1971, Coldea *et al* 1998) and with dynamic scaling theory. The scaling of $S_L^{\perp}(q, \omega)$ itself was tested, and a finite size scaling plot with $z = 1.48$ is shown in figure 11; the data fall upon a single curve, to within the error bars, but for $L = 16$ there are systematic deviations.

*5.3.2. Anisotropic systems.* The effect of uniaxial anisotropy in magnetic systems has been the subject of experimental and theoretical work (Als-Nielsen 1976). As for the isotropic case, where a physical system ($RbMnF_3$) existed which was well described by this model, there are good physical realizations for anisotropic models: $MnF_2$ (Heller *et al* 1971) and $FeF_2$ (Schulhof *et al* 1971a, Hutchings *et al* 1972) which are well described by this model with weak and strong single-site uniaxial anisotropy respectively. The degree of anisotropy can be found from the ratio of the spin-wave peak energy at the zone centre to that at the zone boundary, and has been found to be 0.17 for $MnF_2$ and 0.66 for $FeF_2$. Theoretical studies of the effect of single-site anisotropy on the classical three-dimensional Heisenberg system (Lovesey and Balcar 1995) predict that the dynamic structure factor will display a strong diffusive longitudinal component and a suppressed propagative transverse component. $S_L^{\perp}(q, \omega)$ should be non-critical in nature, tending to a constant value in the limit $q \to 0$, and $S_L^{\parallel}(q, \omega)$ should be critical with a predicted dynamic critical exponent $z \approx 2$; the renormalization group predicts $z \approx 2.19$ (Hohenberg and Halperin 1977).

Simulations were performed (Landau *et al* 1998) with anisotropies appropriate to each system so that both statics and dynamics could be compared with existing theory and experiment. In the limit of $q \to 0$ three quantities may be measured by experiment, theory and

simulation, i.e. the halfwidth of the dynamic structure factor when fitted to a central Lorentzian, the relaxation rate and the value of the characteristic frequency, respectively. If the component of $S(q, \omega)$ being measured is non-critical then all three of these will converge to a constant value as $q \rightarrow 0$. If it is critical then all three of these will approach a power decay, with the rate given by $z$, the dynamic critical exponent. $L \times L \times L$ body-centred-cubic lattices with periodic boundary conditions were simulated for $20 \leqslant L \leqslant 46$. Hybrid Monte Carlo methods were used to generate initial states, and the critical temperatures were accurately determined: for $D = 1.324$ ($FeF_2$), $J/kT_c = 0.439$; and for $D = 0.0591$ ($MnF_2$), $J/kT_c = 0.478$. The spin dynamics techniques discussed earlier were then used to study the dynamic behaviour. For the highly anisotropic system this correlation time was very large, and the spin dynamics simulation then consumed enormous computer resources due to the large number of MC steps needed to produce new equilibrium configurations.

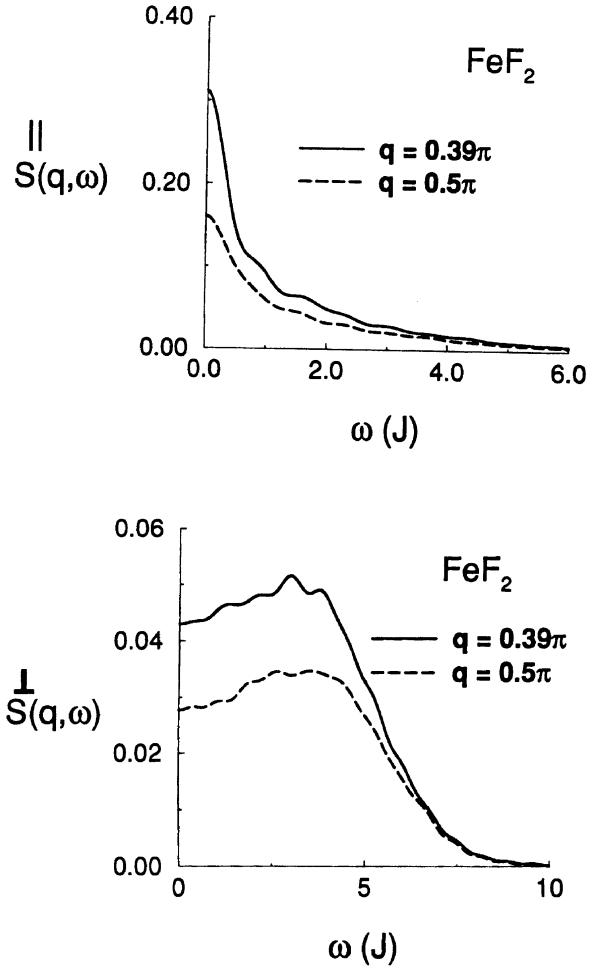


(*a*)

**Figure 14.** Dynamic structure factor for an anisotropic Heisenberg antiferromagnet: (*a*) spin dynamics data at $T_N$; (*b*) neutron scattering data for $FeF_2$ (Hutchings *et al* 1972).

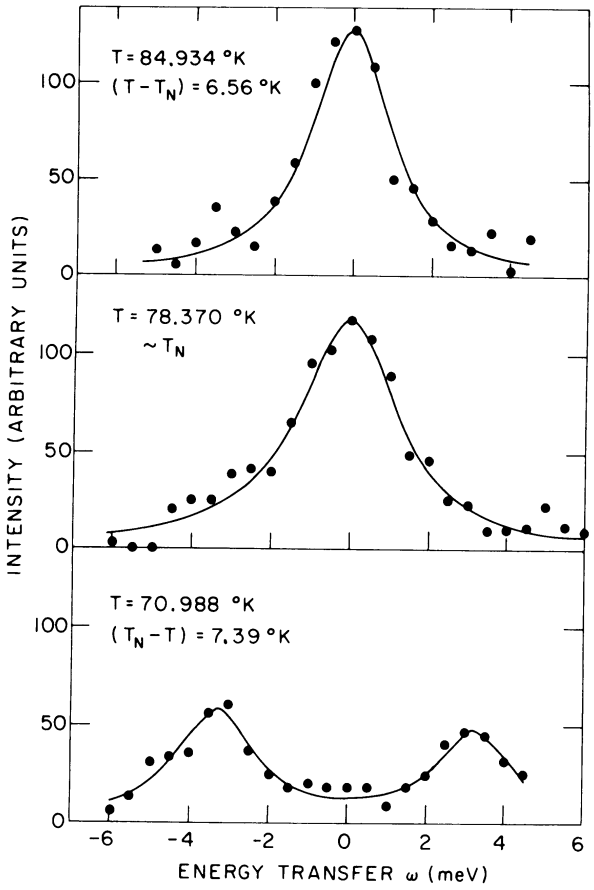


(*b*)

**Figure 14.** (Continued)

The low temperature data showed quite pronounced spin-wave peaks, the locations of which provided good estimates for the dispersion relations. The predictions of linear spin-wave theory ($T = 0$) agree well, although even at this low temperature there is a very slight energy renormalization, particularly for large $q$.

Initial results from the spin dynamics at $T_c$ for the large anisotropy case indicated that the longitudinal component of $S^{\parallel}(q, t)$ had a much longer relaxation time than in the isotropic case, so the study of the low $q$ behaviour was intractable (it would require $t_{max} > 1000/J$). The data, see figure 14, reveal only a central peak in $S_L^{\parallel}(q, \omega)$ indicating purely dissipative behaviour. A comparison of the data for $S_L^{\parallel}(q, \omega)$ with those for $S_L^{\perp}(q, \omega)$ show that the longitudinal component is much more intense, in agreement with both existing theory and experiment results. The transverse component has a short relaxation time so $S_L^{\perp}(q, \omega)$ could be measured over the full range of $q$ values using a very short $t_{max} = 8/J$. (Such a small value was chosen because of the large quantity of computer time required by the MC part of the spin dynamics simulation of the highly anisotropic case.) For $20 \leqslant L \leqslant 46$ the characteristic frequency for the transverse component approaches a constant value with increasing $L$ in the limit of small $q$, indicating non-critical behaviour. The shape of $S_L^{\perp}(q, \omega)$ shows a spin-

wave peak, with the possible addition of a small central peak. These findings are in general agreement with theory and experiment. Neutron scattering data for the transverse component for $FeF_2$ (Hutchings *et al* 1972) show only a central peak at the Néel temperature and yield a value of $z = 2.1 \pm 0.2$. With such large error bars this estimate cannot decide between competing theoretical predictions. Note that $z \sim 2.04$ for (Metropolis) critical relaxation in the anisotropic limit, the 3D Ising model (Wansleben and Landau 1991, Kikuchi and Ito 1993).

Preliminary spin dynamics simulation results for the case of weak anisotropy ($MnF_2$) show purely dissipative behaviour only at low $q$ values of the longitudinal component of $S(q, \omega)$. This indicates crossover to isotropic behaviour due to the weak nature of the anisotropy. The transverse component shows stronger propagative excitations than in the case of stronger anisotropy. This is to be expected since the transverse excitations in the isotropic case are much stronger than those of the strongly anisotropic case. Although not yet complete, these simulational data already show the resolution needed to extract useful information from the dynamic structure factor. With anisotropy present the longitudinal component of the dynamic structure is purely dissipative and the transverse component is non-critical with a weakened spin wave peak. Neutron scattering data for the transverse component for $MnF_2$ (Schulhof *et al* 1971b) shows non-critical behaviour at $T_N$. The longitudinal relaxation rate suggests that $z = 3/2$, consistent with an isotropic system instead of that predicted for an anisotropic model, although the authors express concern that they cannot really access the small $\boldsymbol{q}$ regime and may still be outside the asymptotic critical regime. If this is true, it means that there are not yet sufficiently accurate results from either simulation or experiment to test theoretical predictions.

## 6. Summary and conclusions

Spin dynamics simulations have now become a mature method for probing the time dependent behaviour of magnetic systems. The combination of sophisticated Monte Carlo methods to generate initial states and of high power time integration techniques makes it possible to study larger systems to much longer times than ever before. Indeed, in some cases the spin dynamics data exceed the resolution of real experiments. The picture which is emerging is one in which the general features, including dynamic critical exponents, are correctly predicted by theory. Line shapes and intensities, however, are generally predicted poorly by theory. In some cases there are good experimental data for testing dynamic critical behaviour, but for the most part lineshapes are still known with only modest accuracy. Other challenges remain to be addressed by spin dynamics. For example, there are theoretical predictions for the dynamics near multicritical points (Dohm 1983, Huber 1982) which remain to be tested. The newly developed approach of higher order decomposition time integration methods promises to extend the utility of the method still further.

## Acknowledgments

This work was supported by NSF grant No DMR-9405354. M Krech acknowledges support through the Heisenberg program of the Deutsche Forschungsgemeinschaft.

## References

Allroth E and Mikeska H J 1981a *J. Phys. C: Solid State Phys.* **13** L725
——1981b *Z. Phys.* B **43** 209
Als-Nielsen J 1976 *Phase Transitions and Critical Phenomena* ed C Domb and M Green (New York: Academic)

Balucani U, Carra P, Lovesey S W, Pini M G and Tognetti V 1987 *J. Phys. C: Solid State Phys.* **20** 3953
Bausch R, Janssen H K and Wagner H 1976 *Z. Phys.* **24** 113
Böni P, Chen M E and Shirane G 1987 *Phys. Rev.* B **35** 8449
Böni P and Shirane G 1986 *Phys. Rev.* B **33** 3012
Bramwell S T, Hutchings M T, Norman J, Pynn R and Day P 1988 *J. Physique Coll.* **49** (C8) 1435
Bunker A, Chen K and Landau D P 1996 *Phys. Rev.* B **54** 9259
Burden R L, Faires J D and Reynolds A C 1981 *Numerical Analysis* (Boston: Prindle, Weber and Schmidt)
Chaudhury R and Shastry B S 1988 *Phys. Rev.* B **37** 5216
Chen K, Ferrenberg A M and Landau D P 1993 *Phys. Rev.* B **48** 3249
Chen K and Landau D P 1994 *Phys. Rev.* B **49** 3266
Coldea R, Cowley R A, Perring T G, McMorrow D F and Roessli B 1998 *Phys. Rev.* B **57** 5281
Costa J E R and Costa B V 1996 *Phys. Rev.* B **54** 994
Costa B V, Costa J E R and Landau D P 1997 *J. Appl. Phys.* **81** 5746
Cox U J, Cowley R A, Bates S and Cussen L D 1989 *J. Phys.: Condens. Matter* **1** 3031
Cuccoli A, Lovesey S W and Tognetti V 1994 *J. Phys.: Condens. Matter* **6** 7553
Cuccoli A, Tognetti V and Lovesey S W 1989 *Phys. Rev.* B **39** 2619
Dohm V 1983 *Multicritical Phenomena* ed R Pynn and A Skjeltorp (New York: Plenum) p 81
Evertz H G and Landau D P 1996 *Phys. Rev.* B **54** 12302
Ferrell R A, Menyhárd N, Schmidt H, Schwabl F and Szépfalusy P 1967 *Phys. Rev. Lett.* **18** 891
Freedman R and Mazenko G F 1976 *Phys. Rev.* B **13** 4967
Frey E and Schwabl F 1994 *Adv. Phys.* **43** 577
Gerling R W and Landau D P 1984 *Magnetic Excitations and Fluctuations* ed S W Lovesey *et al* (Berlin: Springer) p 61
——1990 *Phys. Rev.* B **41** 7139
——1992 *J. Magn. Magn. Mater.* **104–107** 246
Gouvêa M E, Mertens F G, Bishop A R and Wysin G M 1990 *J. Phys. C: Solid State Phys.* **2** 1853
Gouvêa M E and Wysin G M 1997 *Phys. Rev.* B **56** 14 192
Gouvêa M E, Wysin G M, Bishop A R and Mertens F G 1989 *Phys. Rev.* B **39** 11 840
Gupta R and Baillie C F 1992 *Phys. Rev.* B **45** 2883
Halperin B I and Hohenberg P C 1967 *Phys. Rev. Lett.* **19** 700
Heller P, Schulhof M P, Nathans R and Linz A 1971 *J. Appl. Phys.* **42** 1258
Hohenberg P C and Halperin B I 1977 *Rev. Mod. Phys.* **49** 435
Huber D L 1978 *Phys. Lett.* A **68** 125
——1982 *Phys. Rev.* B **26** 3758
Hutchings M T, Day P, Janke E and Pynn R 1986 *J. Magn. Magn. Mater.* **54–57** 673
Hutchings M T, Schulhof M P and Guggenheim H J 1972 *Phys. Rev.* B **5** 154
Janke W and Nather K 1993 *Phys. Rev.* B **48** 7419
Kawabata C, Takeuchi M and Bishop A R 1986 *J. Magn. Magn. Mater.* **54–57** 871
Kawasaki K 1976 *Phase Transitions and Critical Phenomena* vol 5a, ed C Domb and M S Green (New York: Academic) p 165
Kikuchi M and Ito N 1993 *J. Phys. Soc. Japan* **62** 3052
Kjems J K and Steiner M 1978 *Phys. Rev. Lett.* **41** 1137
Kosterlitz J M and Thouless D J 1973 *J. Phys. C: Solid State Phys.* **6** 1181
Krech M, Bunker A and Landau D P 1998 *Comp. Phys. Commun.* **111** 1
Landau D P 1990 *Finite Size Scaling and Numerical Simulation of Statistical Systems* ed V Privman (Singapore: World Scientific) p 223
——1992 *Monte Carlo Simulations in Condensed Matter Physics* ed K Binder (Heidelberg: Springer) p 23 and references therein
Landau D P, Chen K and Bunker A 1998 *J. Magn. Magn. Mater.* at press
Landau D P and Gerling R W 1992 *J. Magn. Magn. Mater.* **104–107** 843
Lindgård P A 1983 *Phys. Rev.* B **27** 2980
Lovesey S W 1984 *Theory of Neutron Scattering from Condensed Matter* (Oxford: Clarendon)
Lovesey S W and Balcar E 1995 *J. Phys.: Condens. Matter* **7** 2147
Lovesey S W and Williams R D 1986 *J. Phys. C: Solid State Phys.* **19** L253
Menezes S L, Pires A S T, and Gouvêa M E 1992 *Phys. Rev.* B **45** 10 454
——1993 *Phys. Rev.* B **47** 12 280
Mertens F G, Bishop A R, Gouvêa M E and Wysin G M 1988 *J. Physique Coll.* **49** (C8) 1385
Mertens F G, Bishop A R, Wysin G M and Kawabata C 1987 *Phys. Rev. Lett.* **59** 117

——1989 *Phys. Rev.* B **39** 591
Mikeska H J 1978 *J. Phys. C: Solid State Phys.* **11** L29
Moussa F and Villain J 1976 *J. Phys. C: Solid State Phys.* **9** 4433
Nelson D R and Fisher D S 1977 *Phys. Rev.* B **16** 4945
Nelson D R and Kosterlitz J M 1977 *Phys. Rev. Lett.* **39** 1201
Peczak and Landau D P 1993 *Phys. Rev.* B **47** 14 260
Pereira A R, Pires A S T, Gouvêa M E and Costa B V 1992 *Z. Phys.* B **89** 109
Regnault L P, Rossat-Mignod J, Henry J Y and de Jongh L J 1983 *J. Magn. Magn. Mater.* **31–34** 1205
Schulhof M P, Hutchings M T and Guggenheim H J 1971a *J. Appl. Phys.* **42** 1376
Schulhof M P, Nathans R, Heller P and Linz A 1971b *Phys. Rev.* B **4** 2254
Staudinger M, Gerling R W and Landau D P 1985 *J. Appl. Phys.* **57** 3335
Suzuki M and Umeno K 1993 *Computer Simulation Studies in Condensed Matter Physics VI* ed D P Landau *et al* (Berlin: Springer) p 74
Swendsen R W, Wang J-S and Ferrenberg A M 1992 *Monte Carlo Simulations in Condensed Matter Physics* ed K Binder (Heidelberg: Springer) p 75 and references therein
Thoma S, Frey E and Schwabl F 1991 *Phys. Rev.* B **43** 5831
Tobochnik J and Chester G V 1979 *Phys. Rev.* B **20** 3761
Tucciarone A, Lau H Y, Corliss L M, Delapalme A and Hastings J M 1971 *Phys. Rev.* B **4** 3206
Villain J 1974 *J. Physique* **35** 27
——1975 *J. Physique* **36** 581
Völkel R, Mertens F G, Bishop A R and Wysin G M 1991a *Phys. Rev.* B **43** 5992
Völkel R, Wysin G M, Bishop A R and Mertens F G 1991b *Phys. Rev.* B **44** 10 066
Wagner H 1970 *Phys. Lett.* A **33** 58
Wansleben S and Landau D P 1991 *Phys. Rev.* B **43** 6006
Watson R E, Blume M and Vineyard G H 1969 *Phys. Rev.* **181** 811
Wiesler D G, Zabel H and Shapiro S M 1994 *Z. Phys.* B **93** 297
Wysin G M 1990 *Computational Physics and Cellular Automata* ed A Pires, D P Landau D P and H J Herrmann (Singapore: World Scientific) p 29
Wysin G M, Gouvêa M E, Bishop A R and Mertens F G 1988 *Computer Simulation Studies in Condensed Matter Physics: Recent Developments* ed D P Landau, K K Mon and H-B Schuettler (Heidelberg: Springer) p 40
Young A P and Shastry B S 1982 *J. Phys. C: Solid State Phys.* **15** 4547